European Journal of Mechanics / A Solids 117 (2026) 105988

Contents lists available at ScienceDirect

European Journal of Mechanics / A Solids

journal homepage: www.elsevier.com/locate/ejmsol

Full length article

A finite-strain chemo-electro-mechanical model for gel polymer electrolytes with dynamic ion exchange between fluid and polymer phases

Mattia Serpelloni [a,*], Alberto Salvadori [a], Luigi Cabras [b,c]

[a] Department of Mechanical and Industrial Engineering, Università degli Studi di Brescia, via Branze 38, Brescia 25123, Italy
[b] Department of Engineering and Architecture, University of Trieste, via Valerio 6/1, Trieste 34127, Italy
[c] Center for Energy, Environment and Transport Giacomo Ciamician, University of Trieste, Trieste, Italy

ARTICLE INFO

Keywords:
Multiphysics
Modeling and simulations
Gel polymer electrolytes
Large strains thermomechanics of continua
Finite elements

ABSTRACT

Climate change pivots on shifting to renewable energy sources and to reliable, readily available energy storage systems; at present, lithium-ion batteries (LiBs) are the most advanced industrial technology. Great efforts towards novel materials are underway to overcome well known safety concerns in conventional liquid electrolytes. Gel polymer electrolytes (GPEs) are promising candidates. They are composed of a fluid mixture that fills the interstitial spaces in a solid polymer network. The confined liquid boosts the conductivity and improves the surface contact with electrodes. We devise a multiphysics model for GPEs, framed in the finite-strains thermo-mechanics of continua. It accounts for the electro-chemistry, transport, and mechanics of energy storage. Predictive science is achieved through simulations of the transport and chemical interactions of solvent and ions during material advection. Insightful information on the behavior of GPE during charge–discharge of (Li-ion) batteries are attained.

1. Introduction

A great effort to replace conventional liquid electrolytes in LiBs with novel materials with enhanced transport properties, good mechanical strength, low interfacial resistance, and increased safety, is underway (Serpelloni et al., 2024). Solid-state polymer electrolytes (SPE) (Esmizadeh et al., 2024) have been considered a promising solution. In spite of the recent developments, challenges such as low ionic conductivity at room temperature as well as poor contact with the electrodes remain unsolved; gel polymer electrolytes (GPEs) are attractive since soaking the polymer matrix in a liquid electrolyte enhances the conductivity and improves the adhesion to electrodes (Zhu et al., 2019). GPEs are, in addition, a serious candidate when mechanical flexibility (Deb, 2024) and high-performances are required, ensuring the feasibility of up-scaling (Castillo et al., 2021; Wei et al., 2022).

The ionic conduction mechanisms in GPEs are complex and multiple, varying with the composition of the polymer electrolyte. In SPEs, lithium transport is the combination of a sub-diffusive Li^+ motion along polymeric chains, a motion driven by polymer chains, and an inter-segmental Li^+ hopping from one polymer chain to another (Borodin and Smith, 2006). When liquid is present, as in GPEs, it is the major responsible for the ionic conductivity (Baskoro et al., 2019), whereas the mechanical strength is attributed to the polymer matrix. In acrylate-based quasi-solid/gel polymer electrolytes, the activation energy for ionic conduction has been found to be similar to that of liquid electrolytes. Liquid-filled pores do not play a significant role in bulk ionic conductivity. Instead, ionic conduction is predominantly facilitated through the polymer chains and the solvent that surrounds them (Li et al., 2023). Gels are generally characterized by three main mechanisms: swelling (or drying), squeezing, and forced permeation. Swelling is the absorption of a dry gel dipped into a solvent. Squeezing promotes an outward flux of solvent from the sample as a consequence of an applied stress on the gel. Forced permeation occurs when a solvent, on one side of the gel, is pressed by a piston (Doi, 2009).

This paper presents a three-dimensional model for GPEs, framed in the realm of modern continuum mechanics and thermodynamics (Gurtin et al., 2010; Holzapfel, 2001; Tadmor et al., 2011). Mathematical formulations of the multi-physics characterization of elastomeric gels, including hydrogels, have been proposed by several authors (Hong et al., 2008; Hajikhani et al., 2021; Duda et al., 2010; Lucantonio et al., 2013; Chester and Anand, 2010; Anand, 2011; Chester et al., 2015; Narayan et al., 2021; Narayan and Anand, 2022; Haohui et al., 2020; Chen and Zhao, 2022; Xuanhe et al., 2008; Latz and Zausch, 2015; Balo et al., 2017; Chester and Anand, 2011; Chester, 2012; Bacca and McMeeking, 2017; Rossi et al., 2019; Simon and Grzywna, 1992). Anand and Chester developed a theoretical framework in Chester and Anand (2010), Anand (2011), Chester et al.

* Corresponding author.
E-mail address: mattia.serpelloni@unibs.it (M. Serpelloni).

https://doi.org/10.1016/j.euromechsol.2025.105988
Received 28 August 2025; Received in revised form 13 November 2025; Accepted 7 December 2025
Available online 24 December 2025

(2015) for the mechanical behavior of elastomeric gels as well as for poly-electrolyte gels (Narayan and Anand, 2022). A rigorous non-equilibrium thermodynamic framework has been presented in Haohui et al. (2020) to study the coupled deformation and diffusion of polyelectrolyte gels, emphasizing and quantifying cross-diffusion. In Chen and Zhao (2022), a general framework was proposed for deriving constitutive equations for soft elastomers with arbitrary initial states, whereas in Xuanhe et al. (2008) a theory for gels subjected to electromechanical loads was formulated stemming from non-convex free-energy functions.

Thermal effects are relevant for GPEs (Latz and Zausch, 2015), and their high thermal stability has been highlighted in Balo et al. (2017). A model for thermally responsive swelling of gels has been proposed in Chester and Anand (2011). Further multiphysics models for gels have been provided in Chester (2012), Bacca and McMeeking (2017) coupling fluid permeation and large viscoelastic deformation of polymeric gels.

Key points of the present study. We propose a multi-physics and multiscale compatible[1] model for GPEs through the interplay of a fluid mixture (solvent and a LiX salt solute) with a polymer solid network. Stemming from experimental evidences (Gerdroodbar et al., 2023; Ford et al., 2020; He et al., 2024) we explicitly account for the dynamic exchange between the ionic transport in the fluid and in the polymer network, by means of tailored chemical reactions. The chemo-transport-mechanical response of the GPE emerges from a rigorous thermodynamic description of the several multiphysics interactions between ions moving across the solid network and through the liquid phase of the gel (Li et al., 2023; Saito et al., 2003). The mechanical coupling between the solvent and the polymer network has been formulated in the framework of finite strains, adopting the Maxwell–Stefan approach to write a set of constitutive relations between the fluxes of species and their thermodynamic gradients. Therefore, the novelty of our contribution lies in the explicit treatment of ionic transport across both liquid and polymeric phases, supported by tailored reaction terms and into a new thermodynamically consistent formulation in the realm of finite-strain mechanics. Numerical simulations, conducted under the assumption of thermal equilibrium, demonstrate how the selected material parameters influence ion concentration, electric potential, and deformation — showing behavior consistent with Maxwell–Stefan transport theory. Moreover, the results offer theoretical insights that may guide future experimental investigations.

The manuscript is organized as follows. Notation and nomenclature are defined in Section 2, while the reactions kinetics and mechanical kinematics of the GPE are described in Section 3. The paper follows a nowadays classical theoretical framework inherited from the rational thermo-mechanics of continua (Gurtin et al., 2010): the balance of mass, charge, momentum, and Maxwell's equations have been stated in Section 4, the thermodynamic setting (balance of energy, entropy, Clausius–Duhem inequality, Coleman–Noll procedure in terms of Helmholtz free energy) in Section 5, and the constitutive equations in Section 6. Eventually, the governing equations have been summarized in Section 7 in their strong form. They have been implemented into a finite element code, using the COMSOL Multiphysics Finite Element Software. Outcomes of numerical simulations, triggered by an applied current at different operative conditions, have been detailed and compared in Section 8, highlighting the most relevant features of GPE based batteries. The conclusions drawn after the numerical approximation of the model pave the way to devoted experimental campaigns on GPE cells.

[1] Multiscale approaches need energy conservation through the scale transitions. In the case of batteries, we must ensure that all types of energy are conserved, including the electromagnetic contribution, which would be lacking in the case of imposition a priori of the electroneutrality condition of the electrolyte (Cabras et al., 2022; Salvadori et al., 2015a).

Table 1
Notation adopted for tensor, vector, and scalar fields both for current and reference configuration.

Variables and values	Reference configuration	Current configuration
2-nd order tensor	$\mathbf{A}$	$\mathbf{a}$
vector	$\vec{A}$	$\vec{a}$
scalar	a_R	a

Table 2
Notation adopted for the differential operators in current and reference configuration.

Operators	Reference configuration	Current configuration
divergence	Div [ ]	div [ ]
gradient	Grad [ ]	grad [ ]
curl	Curl [ ]	curl [ ]

2. Notation and nomenclature

We adopt uppercase fonts for referential $\overrightarrow{VECTOR}$ and **TENSOR** fields, and lower case fonts for $\overrightarrow{vector}$ and **tensor** in the current configuration (see Table 1). Concerning scalar fields, we embrace the notation of Gurtin et al. (2010), where referential scalar fields are identified through a lowercase letter with a subscript $_R$. Indeed, uppercase letters typically denote material parameters (e.g. the shear modulus G), or customary different scalar fields (e.g. temperature T versus time t) (Bonanno et al., 2023).

Symbols adopted for divergence, gradient, and curl operators, in current and reference configurations, are summarized in Table 2. Scalar product for vectors and tensors (double index contraction) are defined by the symbols $\cdot$ and $:$, respectively, whereas $\times$ denotes cross product.

The partial time derivative of a generic field φ (scalar, vector, or tensor) will be denoted as $\frac{\partial \varphi}{\partial t}$, whereas the total derivative will be denoted as $\frac{d\varphi}{dt}$. The mass flux of species α is denoted with $\vec{h}_\alpha$. Spatial fields are defined in space $\vec{x}$ and time $0 \le t \le t_f$. Functional dependence, however, is specified only when necessary to enhance readability.

3. Kinetics and kinematics

Consider a GPE made by a polymer (P) and a fluid mixture composed by a solvent (S) with solute species (Li^+ and X^-) dissolved in it. Li^+ are transported both across the polymer chains (via segmental motion, hopping or channeling mechanism, see for instance (Gerdroodbar et al., 2023)) and in the liquid phase (Salvadori et al., 2015b). We denote with Li_f^+ the lithium ions that emanate from the complete dissociation of a generic salt LiX and move within the solvent together with anionic species X^-. Lithium ions transported along the polymer network will be denoted with Li_p^+. They have affinity with immobile charges (A^-) which grant electroneutrality. The attitude of ions to be transported in the polymer network is modeled via the chemical reaction

$$\mathrm{LiA} \underset{k_b^{(1)}}{\overset{k_f^{(1)}}{\rightleftarrows}} \mathrm{Li_p^+} + \mathrm{A^-}\,, \tag{1}$$

where $k_f^{(1)}$ and $k_b^{(1)}$ are the forward and backward rate constants for the reaction (1), respectively. Only in cases where the solubility of ions in the polymer is near zero (such as in polyvinylidene difluoride (PVDF) gel electrolyte swelled with typical liquid electrolyte with lots of carbonate solvent) is the polymer phase inactive for ion transport and just providing mechanical support. In those cases $k_f^{(1)}$ vanishes.

A thorough investigation on the effect of solvent in GPEs was carried out in Gerdroodbar et al. (2023), He et al. (2024), showing that the ionic conductivity of a GPE is improved when a less polar polymer is used since a lower fraction of the ions are coordinated with the

polymer chain at any point in time. The mechanisms responsible for the enhanced conductivity was elucidated in Ford et al. (2020): decreasing Li^+-polymer interactions and gel solvent-polymer interactions leads to an increase in Li^+ mobility. This evidence suggests that ions can move between the polymer coordinated state and the solvent coordinated state. In any case where the gel electrolyte contains a polar polymer (like polyethylene oxide (PEO)) that is able to solvate Li^+, there will be some fraction of ions that has all or part of the coordination shell that is made of the polar polymer segment rather than a small solvent molecule. However the residence time in any state is really short, and the ion can attach and detach from the polymer chains. We describe such dynamic interaction between the fluid/solid ionic transport by a further reaction

$$\mathrm{Li}^+_{\mathrm{p}} \underset{k_b^{(2)}}{\overset{k_f^{(2)}}{\rightleftarrows}} \mathrm{Li}^+_{\mathrm{f}} \,, \tag{2}$$

which governs the influence of the fluid electrolyte on the polymeric transport and vice-versa. $k_f^{(2)}$ and $k_b^{(2)}$ are the rate constants for reaction (2). The two ionic transport mechanisms are uncorreleted when $k_f^{(2)} = k_b^{(2)} = 0$. The reaction rates for reactions (1) and (2) will be denoted with $\mathrm{w}_{\mathrm{R}}^{(1)}$ and $\mathrm{w}_{\mathrm{R}}^{(2)}$, respectively.

The GPE is idealized as a continuum body embedded in an Euclidean space E^3 (Hajikhani et al., 2021). Let Ω_0 and Ω_t be the referential and current configurations of the GPE during its motion, respectively: Ω_0 corresponds to the dry state, without solvent and solutes (Doi, 2009; Narayan and Anand, 2022). Denote with $\vec{x} \in \Omega_t$ the image of $\vec{X} \in \Omega_0$ at a given time t through a "sufficiently smooth" function $\vec{\chi}(\vec{X}, t)$ called motion (Gurtin et al., 2010). Define with

$$\mathbf{F} = \mathrm{Grad}\left[\vec{x}\right] = \partial\vec{\chi}/\partial\vec{X}$$

the deformation gradient, and assume that $J = \det[\mathbf{F}] > 0$.

We model the GPE as a Larché-Cahn system (Simon and Grzywna, 1992), assuming that the material volumes for the gel and the polymer network coincide, identifying the velocity of the polymer ($\vec{v}_p$) with the advection velocity, i.e., $\vec{v}_p = \vec{v}_{\mathrm{adv}} = d\vec{x}/dt$ (Doi, 2009). For a generic scalar, vector, or tensor field $\varphi = \varphi(\vec{\chi}(\vec{X}, t), t)$, total time derivative becomes

$$\frac{d\varphi}{dt} = \frac{\partial\varphi}{\partial t} + \mathrm{grad}[\varphi] \cdot \vec{v}_{\mathrm{adv}} \,.$$

The *molar* mass flux of any component α of the fluid mixture reads (Ganser et al., 2019)

$$\vec{h}_\alpha = c_\alpha \left(\vec{v}_\alpha - \vec{v}_{\mathrm{adv}}\right) \,,$$

where $\vec{v}_\alpha$ is termed the velocity of convection of the species α.

As in Ganser et al. (2019), define with $\mathcal{P}_t^\alpha$ a control volume for the species α and with $\mathcal{P}_t$ a control volume for the hosting material. The velocity of species $\vec{v}_\alpha(\vec{x}, t)$ in $\mathcal{P}_t^\alpha$ is related to the advection of $\mathcal{P}_t$ by Reynold's Theorem

$$\frac{d}{dt}\int_{\mathcal{P}_t^\alpha} \varphi_\alpha \, d\mathrm{v}_\alpha = \frac{d}{dt}\int_{\mathcal{P}_t} \varphi_\alpha \, d\mathrm{v} + \int_{\partial\mathcal{P}_t} \mu_\alpha^\varphi \, \vec{h}_\alpha \cdot \vec{n} \, d\mathrm{a} \,, \tag{3}$$

having defined $\mu_\alpha^\varphi = \varphi_\alpha / c_\alpha$ as in Arricca et al. (2023). Exploiting Nanson's formula (see Supplementary Material, *Section 1.1.1. Mathematical tools from continuum mechanics*) Eq. (3) can be recasted in the reference configuration as

$$\frac{d}{dt}\int_{\mathcal{P}_t^\alpha} \varphi_\alpha \, d\mathrm{v}_\alpha = \int_{\mathcal{P}_0} \frac{d\varphi_{\mathrm{R}}^\alpha}{dt} \mathrm{dV} + \int_{\partial\mathcal{P}_0} \mu_\alpha^\varphi \, \vec{H}_\alpha \cdot \vec{N} \, dA \,, \tag{4}$$

where

$$\vec{H}_\alpha = J\,\mathbf{F}^{-1}\,\vec{h}_\alpha \,, \qquad \varphi_{\mathrm{R}}^\alpha = J\,\varphi^\alpha \,. \tag{5}$$

In the so called Larché-Cahn formulation, the hosting polymer network is organizes an elastic response in reaction to the inelastic contributions given by the inlet or outlet of the fluid mixture inside the polymer matrix. The multiplicative decomposition

$$\mathbf{F} = \mathbf{F}^e\mathbf{F}^s$$

is a modeling strategy that allows to account for mechanical swelling and shrinking due to diffusion of species (Chester and Anand, 2010; Narayan and Anand, 2022). It is broadly used (Chester and Anand, 2010; Narayan and Anand, 2022; Lucantonio et al., 2013; Hajikhani et al., 2021) for polymer gels, although different approaches have been developed in Doi (2009), Bacca and McMeeking (2017). $\mathbf{F}^s$ accounts for the swelling deformations due to absorption and dis-absorption, whereas $\mathbf{F}^e$ for the elastic deformations, given by the recoverable polymer network distortion that makes deformations compatible (Bucci et al., 2016).

Adopting an isotropic description of the mechanism of expansion/contraction of the gel due to the solvent, $\mathbf{F}^s = J_s^{1/3}\mathbf{1}$, we can deduce the following identities

$$\mathbf{C}^e = \mathbf{F}^{eT}\mathbf{F}^e \,, \qquad \mathbf{C} = J_s^{2/3}\mathbf{C}^e \,, \qquad \mathbf{C}^s = J_s^{2/3}\mathbf{1}. \tag{6}$$

It is assumed that the volume change induced by swelling/shrinking is isotropic and results solely from variations in solvent content (Narayan and Anand, 2022). Accordingly,

$$J_s = 1 + \Omega_{\mathrm{S}}\left(c_{\mathrm{R}}^{\mathrm{S}} - c_{\mathrm{R}}^{\mathrm{S0}}\right) \,,$$

with Ω_{S} the molar volume of the solvent and $c_{\mathrm{R}}^{\mathrm{S0}}$ the concentration of solvent associated to the undeformed referential configuration. In agreement with (Holzapfel, 2001; Simo and Hughes, 1998), the elastic deformation gradient is multiplicatively decomposed into a volumetric $\mathbf{F}^{e^v} = J_e^{1/3}\mathbf{1}$ and an isochoric $\mathbf{F}^{e^i}$ part, with $\det[\mathbf{F}^{e^i}] = 1$, as common in the realm of visco-elasticity (Holzapfel, 2001; Simo and Hughes, 1998).

4. Balance equations

Balance equations are stated for mass, charge, linear as well as angular momentum, energy, and entropy, together with Maxwell's equations under quasi-electrostatic conditions, which can be interpreted as balance equations, too Müller et al. (2022). In these equations, we select the following thermodynamic state variables: displacements $\vec{U}$; electric potential ϕ; concentrations, i.e., the number of moles per unit volume, of species S, Li^+_f, X^-, Li^+_p, A^-, LiA. $c_{\mathrm{Li}^+_{\mathrm{f}}}$ and $c_{\mathrm{Li}^+_{\mathrm{p}}}$ denote the concentrations of mobile Li^+ ions, c_{LiA} the concentration of polymer chains, c_{A^-} the concentration of negative counterparts in the polymer, c_{X^-} the concentration of negative ions in the solvent, and c_{S} the concentration of the solvent in the gel.

4.1. Mass balance equations

The hosting material in our Larché-Cahn formulation has been identified with the polymer, with spatial density ρ^{p} and referential density $\rho_{\mathrm{R}}^{\mathrm{p}} = \rho^{\mathrm{p}} J$. The referential mass balance equation for the polymer reads:

$$\frac{d}{dt}\rho_{\mathrm{R}}^{\mathrm{p}} = 0. \tag{7}$$

In view of Eq. (1), the transport of $\mathrm{Li}^+_{\mathrm{p}}$ leaves immobile, uncompensated charges A^- in the polymer network. Since a polymer chain LiA potentially transforms in immobile A^-, the concentration sum $c_R^{\mathrm{LiA}} + c_R^{\mathrm{A}^-}$ is a constant, which equals the initial referential concentration c_0 of non-dissociated LiA. The referential mass balance equations read:

$$\frac{d}{dt}c_R^{\mathrm{S}} + \mathrm{Div}\left[\vec{H}_S\right] = s_R^{\mathrm{S}} \,, \tag{8a}$$

$$\frac{d}{dt}c_R^{\mathrm{LiA}} + \mathrm{w}_{\mathrm{R}}^{(1)} = s_R^{\mathrm{LiA}} \,, \tag{8b}$$

$$\frac{d}{dt}c_R^{\mathrm{A}^-} - \mathrm{w}_{\mathrm{R}}^{(1)} = s_R^{\mathrm{A}^-} \,, \tag{8c}$$

$$\frac{d}{dt}c_R^{\mathrm{Li}^+_{\mathrm{p}}} + \mathrm{Div}\left[\vec{H}_{\mathrm{Li}^+_{\mathrm{p}}}\right] - \mathrm{w}_{\mathrm{R}}^{(1)} + \mathrm{w}_{\mathrm{R}}^{(2)} = s_R^{\mathrm{Li}^+_{\mathrm{p}}} \,, \tag{8d}$$

$$\frac{d}{dt}c_R^{\mathrm{Li_f^+}} + \mathrm{Div}\left[\vec{H}_{\mathrm{Li_f^+}}\right] - \mathrm{w}_{\mathrm{R}}^{(2)} = s_R^{\mathrm{Li_f^+}}\,, \tag{8e}$$

$$\frac{d}{dt}c_R^{\mathrm{X^-}} + \mathrm{Div}\left[\vec{H}_{\mathrm{X^-}}\right] = s_R^{\mathrm{X^-}}\,, \tag{8f}$$

where $\mathrm{w}_{\mathrm{R}}^{(1)}$ and $\mathrm{w}_{\mathrm{R}}^{(2)}$ correspond to the reaction rates of chemical reactions (1) and (2), respectively, whereas s_R^{S}, s_R^{LiA}, $s_R^{\mathrm{A^-}}$, $s_R^{\mathrm{Li_p^+}}$, $s_R^{\mathrm{Li_f^+}}$, and $s_R^{\mathrm{X^-}}$ denote more general source terms that may arise from other physical processes and are not directly associated with reaction kinetics. All mass balance equations can be restated in the abstract formalism[2]

$$\frac{d}{dt}c_R^{\alpha} + \mathrm{Div}\left[\vec{H}_{\alpha}\right] + \mathrm{r}_R^{\alpha} = s_R^{\alpha}, \tag{9}$$

with $\alpha = \mathrm{S}$, LiA, $\mathrm{Li_p^+}$, $\mathrm{A^-}$, $\mathrm{Li_f^+}$, $\mathrm{X^-}$. Here, r_R^{α} stands for the source term associated with chemical reactions in this abstract framework. It is zero in Eqs. (8a) and (8f); equal to $\pm w_R^{(1)}$ in Eqs. (8b), (8c), and $-w_R^{(2)}$ for (8e). Finally, in Eq. (8e), for the species $\mathrm{Li_p^+}$, it becomes $r_R^{\mathrm{Li_p^+}} = -w_R^{(1)} + w_R^{(2)}$. The species LiA and $\mathrm{A^-}$ do not possess any intrinsic motility. Their relocation results from the transport and the reaction of the species that can flow.

4.2. Fundamental connections between current and ions fluxes

Denote with the index $\gamma = \mathrm{Li_p^+}, \mathrm{Li_f^+}, \mathrm{X^-}, \mathrm{A^-}$ the ions in the electrolyte, with z_γ the corresponding valence, and with $\mathbb{F}$ the Faraday's constant. The total referential charge is given by the sum

$$q_{\mathrm{R}} = \mathbb{F}\sum_{\gamma} z_\gamma\, c_{\mathrm{R}}^{\gamma}. \tag{10}$$

The ionic flux of species γ in the current configuration is $\vec{i}_\gamma = \mathbb{F}\, z_\gamma\, \vec{h}_\gamma$ and $\vec{I}_\gamma = J\,\mathbf{F}^{-1}\,\vec{i}_\gamma$ is its referential counterpart. The referential current is the sum

$$\vec{I} = \mathbb{F}\sum_{\gamma} z_\gamma\, \vec{H}_\gamma. \tag{11}$$

4.3. Linear and angular momentum balance equations

Under quasi-static conditions, the referential local form of the balances of linear and angular momentum reads as follows

$$\mathrm{Div}\,[\,\mathbf{P}\,] + \vec{B}_{\mathrm{v}} = \vec{0}\,, \qquad \mathbf{F}\mathbf{P}^T = \mathbf{P}\mathbf{F}^T. \tag{12}$$

This formulation will be adopted in the simulations, see Section 8. For the sake of completeness, we shall mention that the general linear and angular momentum balance equations shall account for the inertia forces associated to the flux of species. For conciseness, details on these equations will be deferred to the Supplementary Material (*Sections 1.1.3. Linear momentum balance equation - 1.1.4. Angular momentum balance equation*) and also Ganser et al. (2019).

4.4. Maxwell's equations

Maxwell's equations, expressed in integral form within the current (spatial) configuration, are given by Kaiser and Menzel (2021):

Gauss's laws: $$\int_{\partial\mathcal{P}_t} \vec{d}\cdot\vec{n}\,da = \int_{\mathcal{P}_t} q\,dv, \qquad \int_{\mathcal{P}_t} \vec{b}_{\mathrm{M}}\cdot\vec{n}\,da = 0\,, \tag{13}$$

Faraday's law of induction: $$\int_{\partial\mathcal{A}_t} \vec{\mathfrak{e}}\cdot d\vec{s} = -\frac{d}{dt}\int_{\mathcal{A}_t} \vec{b}_{\mathrm{M}}\cdot\vec{n}\,da\,, \tag{14}$$

Ampère's circuital law: $$\int_{\partial\mathcal{A}_t} \vec{\mathfrak{h}}\cdot d\vec{s} = \int_{\mathcal{A}_t} \vec{i}\cdot\vec{n}\,da + \frac{d}{dt}\int_{\mathcal{A}_t} \vec{d}\cdot\vec{n}\,da\,, \tag{15}$$

where $\mathcal{A}_t$ is not necessarily a closed surface and $\vec{\mathfrak{e}}$ and $\vec{\mathfrak{h}}$ denote the electromotive and magnetomotive intensities, $\vec{d}$ the electric displacement, $\vec{i}$ the electric current density, q the free charge density, and $\vec{b}_{\mathrm{M}}$ the magnetic flux density (Kaiser and Menzel, 2021). These fields may alternatively be described using the Minkowskian electric and magnetic vectors $\vec{e}$ and $\vec{h}_{\mathrm{M}}$, which relate to their effective counterparts through the convective transformations:

$$\vec{\mathfrak{e}} = \vec{e} + \frac{d}{dt}(\vec{x}\times\vec{b}_{\mathrm{M}})\,, \qquad \vec{\mathfrak{h}} = \vec{h}_{\mathrm{M}} - \frac{d}{dt}(\vec{x}\times\vec{d})\,.$$

.

4.4.1. Referential Maxwell's equations

Maxwell's equations in the reference configuration,[3] under the electro-quasistatic approximation and the assumption that the influence of the medium's velocity on both electric and magnetic fields measurements is negligible ($\vec{\mathfrak{e}} = \vec{e}$ and $\vec{\mathfrak{h}} = \vec{h}$), are expressed using the electric field $\vec{E} = \mathbf{F}^T\vec{e}$ and the electric displacement field $\vec{D} = J\mathbf{F}^{-1}\vec{d}$, following the formulation in Salvadori et al. (2015a).

In view of identity (10), Gauss's law in referential differential form reads

$$\mathrm{Div}\left[\vec{D}\right] = \mathbb{F}\sum_{\gamma} z_\gamma\, c_{\mathrm{R}}^{\gamma}. \tag{16}$$

The Maxwell–Faraday equation (Faraday's law of induction), mathematically depicts how a time-evolving magnetic field generates a time (and spatial) variation of a non-conservative electric field, and vice-versa. Its electro-quasi-static restriction states that the electric field is irrotational

$$\mathrm{Curl}\left[\vec{E}\right] = 0 \;\Rightarrow\; \vec{E} = -\mathrm{Grad}\,[\,\phi\,]\,. \tag{17}$$

Therefore, the electro-quasi-static simplification ultimately allows to depict the whole electro-magnetic scenario in batteries by means of a single scalar function ϕ, i.e., the *electrostatic potential*. A single law rules the evolution of the electric potential field. It can either be Gauss' law (16) itself, as in Carlstedt et al. (2022), or the equation

$$\mathrm{Div}\left[\vec{I} + \frac{d}{dt}\vec{D}\right] = 0\,, \tag{18}$$

which comes out applying the divergence operator to Ampére's law (with Maxwell's correction), as in Salvadori et al. (2015c).

5. Thermodynamics

5.1. Balance of energy

The first law of thermodynamics relies on the Principle of Conservation of Energy. We express it with a balance equation in the current configuration, namely:

$$\frac{d}{dt}\left[\,\mathcal{U}(\mathcal{P}_t) + \mathcal{K}(\mathcal{P}_t)\,\right] = \mathcal{W}_u(\mathcal{P}_t) + \mathcal{Q}_u(\mathcal{P}_t) + \mathcal{T}_u(\mathcal{P}_t) + \mathcal{E}_u(\mathcal{P}_t). \tag{19}$$

It states that the internal energy $\mathcal{U} = \int_{\mathcal{P}_t} u\,dv$ and the kinetic energy $\mathcal{K}$, evaluated over an arbitrary material sub-region $\mathcal{P}_t \subset \Omega_t$, may vary due to interactions with the universe (anything that is not $\mathcal{P}_t$) or because of source terms in $\mathcal{P}_t$ itself (Müller et al., 2022). The external power expenditures are due to various interactions, widely described in Arricca et al. (2023): mechanical $\mathcal{W}_u$, heat transfer and generation $\mathcal{Q}_u$, mass transport and production $\mathcal{T}_u$, and electromagnetic $\mathcal{E}_u$. The electromagnetic contribution is due to the energy flux vector, generated by the electric $\vec{e}$ and magnetizing $\vec{h}_{\mathrm{M}}$ fields

$$\mathcal{E}_u = \int_{\partial\mathcal{P}_t} (\vec{e}\times\vec{h}_{\mathrm{M}})\cdot\vec{n}\,da\,.$$

[2] Insights on the derivations of these equations are provided in Supplementary Material, *Section 1.1.2. Mass balance equations*.

[3] For a detailed discussion, the reader is referred to the Supplementary Material, *Section 1.1.5. Maxwell's equations*.

It is not trivial to recognize $\vec{e}\times\vec{h}_{\mathrm{M}}$ as an energy flux vector, but it actually results from Poyinting's theorem (see also Kovetz (1989), De Groot and Mazur (1984)). The balance of energy writes in extenso as

$$\begin{aligned}&\frac{d}{dt}\int_{\mathcal{P}_t} u_{\mathrm{p}}+\frac{\rho_{\mathrm{p}}}{2}|\vec{v}_{\mathrm{adv}}|^2\,dv+\sum_\alpha\frac{d}{dt}\int_{\mathcal{P}_t^\alpha}u_\alpha+\frac{\rho_\alpha}{2}|\vec{v}_\alpha|^2\,dv_\alpha\\&=\int_{\mathcal{P}_t}s_{\mathrm{q}}\,dv-\int_{\partial\mathcal{P}_t}\vec{q}\cdot\vec{n}\,da+\\&\quad+\int_{\mathcal{P}_t}\vec{b}_{\mathrm{p}}\cdot\vec{v}_{\mathrm{adv}}\,dv+\int_{\partial\mathcal{P}_t}\vec{t}\cdot\vec{v}_{\mathrm{adv}}\,da+\sum_\alpha\int_{\mathcal{P}_t^\alpha}\vec{b}_\alpha\cdot\vec{v}_\alpha+\mu_\alpha^u s_\alpha\,dv_\alpha\\&\quad-\int_{\partial\mathcal{P}_t}(\vec{e}\times\vec{h}_{\mathrm{M}})\cdot\vec{n}\,da.\end{aligned}\tag{20}$$

The referential version of the energy balance (20) in its general form is detailed in the Supplementary Material, *Section 1.1.6. Balance of Energy*, making recourse to the approach developed in Arricca et al. (2023) and to the balance equations in the general form (see Eq. (18) in the Supplementary Materials). Neglecting the contributions of inertia forces, the local form of the referential energy balance reads

$$\frac{du_{\mathrm{R}}}{dt}-\mu_\alpha^u\frac{dc_{\mathrm{R}}^\alpha}{dt}-\mathbf{P}:\frac{d\mathbf{F}}{dt}+\mathrm{Grad}\left[\mu_\alpha^u\right]\cdot\vec{H}_\alpha-\mu_\alpha^u r_{\mathrm{R}}^\alpha-\left(\frac{d\vec{D}}{dt}+\vec{I}\right)\cdot\vec{E}=s_{\mathrm{R}}^{\mathrm{q}}-\mathrm{Div}\left[\vec{Q}\right],\tag{21}$$

where

$$u_{\mathrm{R}}=u_{\mathrm{R}}^{\mathrm{p}}+\sum_\alpha u_{\mathrm{R}}^\alpha$$

is the referential energy of the GPE.

5.2. Balance of entropy

The Second Principle of thermodynamics states that the variation of the internal entropy $\mathcal{S}$ is due to the transfer and generation/annihilation of heat $\mathcal{Q}_\eta$, the transport and production/depletion of mass $\mathcal{T}_\eta$ and the (non-negative) entropy generation ($\mathcal{S}_{irr}$) during irreversible thermodynamic processes

$$\frac{d\mathcal{S}(\mathcal{P}_t)}{dt}=\mathcal{Q}_\eta(\mathcal{P}_t)+\mathcal{T}_\eta(\mathcal{P}_t)+\frac{d\mathcal{S}_{irr}(\mathcal{P}_t)}{dt},\tag{22}$$

on an arbitrarily chosen material sub-region $\mathcal{P}_t\subset\Omega_t$. Implicitly, the non-trivial assumption is made that mechanical and electromagnetic processes involve only energetic interactions (Holzapfel, 2001; Salvadori et al., 2015c; De Groot and Mazur, 1984; Gyftopoulos and Beretta, 2005), i.e., $\mathcal{W}_\eta=\mathcal{E}_\eta=0$.

As discussed for the first time in Arricca et al. (2023), we define with $\mu_\alpha^\eta=\eta_\alpha/c_\alpha$ the specific entropy provided by a unit supply of moles of species α. An immediate way to establish the physical meaning of μ_α^η emanates from the flux of entropy across the boundary $\partial\mathcal{P}_t$ or its referential counterpart $\partial\mathcal{P}_0$. It reads

$$\int_{\partial\mathcal{P}_t}\eta_\alpha\left(\vec{v}_\alpha-\vec{v}_{\mathrm{adv}}\right)\cdot\vec{n}da=\int_{\partial\mathcal{P}_t}\mu_\alpha^\eta\vec{h}_\alpha\cdot\vec{n}da=\int_{\partial\mathcal{P}_0}\mu_\alpha^\eta\vec{H}_\alpha\cdot\vec{N}dA=\int_{\mathcal{P}_0}\mathrm{Div}\left[\mu_\alpha^\eta\vec{H}_\alpha\right]\mathrm{dV}.\tag{23}$$

Deferring again to the Supplementary Material, *Section 1.1.7. Balance of Entropy*, which analyzes the general form of the entropy imbalance in the current configuration, we neglect here the contributions of inertia forces and conclude that the referential global form of the entropy balance (22) reads

$$\int_{\mathcal{P}_0}\frac{d\eta_{\mathrm{R}}}{dt}+\mathrm{Div}\left[\mu_\alpha^\eta\vec{H}_\alpha\right]\mathrm{dV}=\int_{\mathcal{P}_0}\frac{s_{\mathrm{R}}^{\mathrm{q}}}{T}-\mathrm{Div}\left[\frac{\vec{Q}}{T}\right]+\mu_\alpha^\eta s_{\mathrm{R}}^\alpha+\frac{d\eta_{\mathrm{R}}^{\mathrm{irr}}}{dt}\mathrm{dV},\tag{24}$$

where the referential entropy of the GPE is defined as

$$\eta_{\mathrm{R}}=\eta_{\mathrm{R}}^{\mathrm{p}}+\sum_\alpha\eta_{\mathrm{R}}^\alpha.$$

Upon exploiting the mass balance Eq. (8), some algebra leads to the local form of the entropy inequality

$$T\frac{d\eta_{\mathrm{R}}}{dt}-T\,\mu_\alpha^\eta\frac{dc_{\mathrm{R}}^\alpha}{dt}+T\,\mathrm{Grad}\left[\mu_\alpha^\eta\right]\cdot\vec{H}_\alpha-T\,\mu_\alpha^\eta r_{\mathrm{R}}^\alpha-\frac{\mathrm{Grad}\left[T\right]}{T}\cdot\vec{Q}-s_{\mathrm{R}}^{\mathrm{q}}+\mathrm{Div}\left[\vec{Q}\right]\geq 0.\tag{25}$$

5.3. Clausius-Duhem inequality

The Clausius–Duhem inequality (Tadmor et al., 2011) arises subtracting Eqs. (21) from (25). It reads

$$\begin{aligned}&T\frac{d\eta_{\mathrm{R}}}{dt}-\frac{du_{\mathrm{R}}}{dt}+\left(\frac{d\vec{D}}{dt}+\vec{I}\right)\cdot\vec{E}+\frac{dc_{\mathrm{R}}^\alpha}{dt}\left(\mu_\alpha^u-T\mu_\alpha^\eta\right)+r_{\mathrm{R}}^\alpha\left(\mu_\alpha^u-T\mu_\alpha^\eta\right)+\\&\quad+\mathbf{P}:\frac{d\mathbf{F}}{dt}-\frac{1}{T}\mathrm{Grad}\left[T\right]\cdot\vec{Q}-\left(\mathrm{Grad}\left[\mu_\alpha^u\right]-T\,\mathrm{Grad}\left[\mu_\alpha^\eta\right]\right)\cdot\vec{H}_\alpha\geq 0\,.\end{aligned}\tag{26}$$

Such inequality can be restated selecting the Helmholtz free energy

$$\psi_{\mathrm{R}}=u_{\mathrm{R}}-T\eta_{\mathrm{R}}$$

as the thermodynamic potential (McMeeking and Landis, 2005). Furthermore, denote with $\overline{\mu}_\alpha=\mu_\alpha^u-T\mu_\alpha^\eta$ and $\underline{\vec{Q}}=\vec{Q}+T\,\mu_\alpha^\eta\vec{H}_\alpha$ as in Arricca et al. (2023). The Clausius–Duhem inequality eventually writes

$$\begin{aligned}&-\frac{d\psi_{\mathrm{R}}}{dt}-\eta_{\mathrm{R}}\frac{dT}{dt}+\frac{1}{2}\mathbf{S}:\frac{d\mathbf{C}}{dt}+\vec{E}\cdot\frac{d\vec{D}}{dt}+\mu_\alpha\frac{dc_{\mathrm{R}}^\alpha}{dt}-\frac{1}{T}\underline{\vec{Q}}\cdot\mathrm{Grad}\left[T\right]\\&\quad-\mathrm{w}_{\mathrm{R}}^{(1)}\mathrm{A}_{\mathrm{R}}^{(1)}-\mathrm{w}_{\mathrm{R}}^{(2)}\mathrm{A}_{\mathrm{R}}^{(2)}+\\&\quad-\mathrm{Grad}\left[\mu_{\mathrm{S}}\right]\cdot\vec{H}_{\mathrm{S}}-\mathrm{Grad}\left[\overline{\mu}_{\mathrm{Li}_{\mathrm{p}}^+}\right]\cdot\vec{H}_{\mathrm{Li}_{\mathrm{p}}^+}-\mathrm{Grad}\left[\overline{\mu}_{\mathrm{Li}_{\mathrm{f}}^+}\right]\cdot\vec{H}_{\mathrm{Li}_{\mathrm{f}}^+}\\&\quad-\mathrm{Grad}\left[\overline{\mu}_{\mathrm{X}^-}\right]\cdot\vec{H}_{\mathrm{X}^-}\geq 0\,,\end{aligned}\tag{27}$$

where the scalar fields $\overline{\mu}_\alpha$, $\mathrm{A}_{\mathrm{R}}^{(1)}$, $\mathrm{A}_{\mathrm{R}}^{(2)}$ are defined as $\overline{\mu}_\alpha=\mu_\alpha+\mathrm{Fz}_\alpha\phi$, $\mathrm{A}_{\mathrm{R}}^{(1)}=\mu_{\mathrm{A}^-}+\mu_{\mathrm{Li}_{\mathrm{p}}^+}-\mu_{\mathrm{Li}_{\mathrm{A}}}$, and $\mathrm{A}_{\mathrm{R}}^{(2)}=\mu_{\mathrm{Li}_{\mathrm{f}}^+}-\mu_{\mathrm{Li}_{\mathrm{p}}^+}$.

5.4. Coleman and Noll procedure and thermodynamic restrictions

The referential Helmholtz free energy ψ_{R} is taken as a function of temperature T, concentrations c_{R}^α, the right Cauchy–Green tensor $\mathbf{C}$, the electric displacement $\vec{D}$, and of some kinematic internal variables $\boldsymbol{\xi}_m$ that compare with the usual meaning in inelastic constitutive laws.[4] It follows that

$$\frac{d\psi_{\mathrm{R}}}{dt}=\frac{\partial\psi_{\mathrm{R}}}{\partial T}\frac{\partial T}{\partial t}+\frac{\partial\psi_{\mathrm{R}}}{\partial\mathbf{C}}:\frac{\partial\mathbf{C}}{\partial t}+\frac{\partial\psi_{\mathrm{R}}}{\partial c_{\mathrm{R}}^\alpha}\frac{\partial c_{\mathrm{R}}^\alpha}{\partial t}+\frac{\partial\psi_{\mathrm{R}}}{\partial\vec{D}}\cdot\frac{\partial\vec{D}}{\partial t}+\frac{\partial\psi_{\mathrm{R}}}{\partial\boldsymbol{\xi}_m}:\frac{\partial\boldsymbol{\xi}_m}{\partial t}\tag{28}$$

and the Clausius–Duhem inequality (27) becomes

$$\begin{aligned}&-\left(\frac{\partial\psi_{\mathrm{R}}}{\partial T}+\eta_{\mathrm{R}}\right)\frac{\partial T}{\partial t}+\left(\frac{\mathbf{S}}{2}-\frac{\partial\psi_{\mathrm{R}}}{\partial\mathbf{C}}\right):\frac{\partial\mathbf{C}}{\partial t}+\left(\vec{E}-\frac{\partial\psi_{\mathrm{R}}}{\partial\vec{D}}\right)\cdot\frac{\partial\vec{D}}{\partial t}+\left(\mu_\alpha-\frac{\partial\psi_{\mathrm{R}}}{\partial c_{\mathrm{R}}^\alpha}\right)\frac{\partial c_{\mathrm{R}}^\alpha}{\partial t}+\\&\quad-\mathrm{Grad}\left[\mu_{\mathrm{S}}\right]\cdot\vec{H}_{\mathrm{S}}-\mathrm{Grad}\left[\overline{\mu}_{\mathrm{Li}_{\mathrm{p}}^+}\right]\cdot\vec{H}_{\mathrm{Li}_{\mathrm{p}}^+}-\mathrm{Grad}\left[\overline{\mu}_{\mathrm{Li}_{\mathrm{f}}^+}\right]\cdot\vec{H}_{\mathrm{Li}_{\mathrm{f}}^+}-\mathrm{Grad}\left[\overline{\mu}_{\mathrm{X}^-}\right]\cdot\vec{H}_{\mathrm{X}^-}+\\&\quad-\mathrm{w}_{\mathrm{R}}^{(1)}\mathrm{A}_{\mathrm{R}}^{(1)}-\mathrm{w}_{\mathrm{R}}^{(2)}\mathrm{A}_{\mathrm{R}}^{(2)}-\frac{1}{T}\underline{\vec{Q}}\cdot\mathrm{Grad}\left[T\right]-\boldsymbol{\Xi}_m:\frac{d}{dt}\boldsymbol{\xi}_m\geq 0\,.\end{aligned}\tag{29}$$

The internal force, conjugate to $\boldsymbol{\xi}_m$, will be denoted with the symbol $\boldsymbol{\Xi}_m$, i.e.

$$\boldsymbol{\Xi}_m=-\frac{\partial\psi_{\mathrm{R}}}{\partial\boldsymbol{\xi}_m}.\tag{30}$$

Following the Coleman–Noll procedure, the inequality (29) must be satisfied for every admissible process (Tadmor et al., 2011). Assuming

[4] The second-order tensors $\boldsymbol{\xi}_m$ and $\boldsymbol{\Xi}_m$ represent the mth internal (hidden) variable and its energy-conjugate force, respectively. As it has been depicted in Holzapfel (2001), we adopt these variables in order to describe irreversible processes, such as relaxation and creep, in materials that exhibit viscoelastic behavior.

independence of the rates of the independent state variables, the following functional forms for the constitutive relations emerge (Arricca et al., 2023)

$$\eta_{\mathrm{R}} = -\frac{\partial \psi_{\mathrm{R}}}{\partial T}\,, \qquad \mathbf{S} = 2\frac{\partial \psi_{\mathrm{R}}}{\partial \mathbf{C}}\,, \qquad \vec{E} = \frac{\partial \psi_{\mathrm{R}}}{\partial \vec{D}}\,,$$
$$\mu_{\mathrm{A}^-} = \frac{\partial \psi_{\mathrm{R}}}{\partial c_{\mathrm{R}}^{\mathrm{A}^-}}\,, \qquad \mu_{\mathrm{Li_A}} = \frac{\partial \psi_{\mathrm{R}}}{\partial c_{\mathrm{R}}^{\mathrm{Li_A}}}\,,$$
$$\mu_{\mathrm{Li_p^+}} = \frac{\partial \psi_{\mathrm{R}}}{\partial c_{\mathrm{R}}^{\mathrm{Li_p^+}}}\,, \qquad \mu_{\mathrm{S}} = \frac{\partial \psi_{\mathrm{R}}}{\partial c_{\mathrm{R}}^{\mathrm{S}}}\,, \qquad \mu_{\mathrm{Li_f^+}} = \frac{\partial \psi_{\mathrm{R}}}{\partial c_{\mathrm{R}}^{\mathrm{Li_f^+}}}\,, \qquad \mu_{\mathrm{X}^-} = \frac{\partial \psi_{\mathrm{R}}}{\partial c_{\mathrm{R}}^{\mathrm{X}^-}}\,. \tag{31}$$

According to Curie's Principle (De Groot and Mazur, 1984; Castellani and Ismael, 2016), the inequality Eq. (29) splits as follows:

$$\mathrm{w}_{\mathrm{R}}^{(1)}\mathrm{A}_{\mathrm{R}}^{(1)} + \mathrm{w}_{\mathrm{R}}^{(2)}\mathrm{A}_{\mathrm{R}}^{(2)} \le 0\,, \tag{32a}$$
$$\vec{H}_{\mathrm{S}} \cdot \mathrm{Grad}\left[\,\mu_{\mathrm{S}}\,\right] + \vec{H}_{\mathrm{Li_p^+}} \cdot \mathrm{Grad}\left[\,\overline{\mu}_{\mathrm{Li_p^+}}\,\right] + \vec{H}_{\mathrm{Li_f^+}} \cdot + \mathrm{Grad}\left[\,\overline{\mu}_{\mathrm{Li_f^+}}\,\right] + + \vec{H}_{\mathrm{X}^-} \cdot \mathrm{Grad}\left[\,\overline{\mu}_{\mathrm{X}^-}\,\right] + \frac{\vec{Q}}{T} \cdot \mathrm{Grad}\left[\,T\,\right] \le 0, \tag{32b}$$
$$\boldsymbol{\Xi}_m : \frac{d}{dt}\boldsymbol{\xi}_m \le 0. \tag{32c}$$

Owing to the constitutive relations (31), the fields μ_α, $\bar{\mu}_\alpha$, $\mathrm{A}_{\mathrm{R}}^{(1)}$, and $\mathrm{A}_{\mathrm{R}}^{(2)}$ acquire the meaning of chemical potentials, electrochemical potentials, and affinities of the reactions (1) and (2), respectively (Arricca et al., 2023). According to this thermodynamic picture, it appears that μ_α^u and μ_α^η are not partial properties in the conventional thermodynamic sense (Arricca et al., 2023; Gyftopoulos and Beretta, 2005). Specifically,

$$\mu_\alpha^\eta = \frac{\partial \eta_{\mathrm{R}}}{\partial c_{\mathrm{R}}^\alpha} = -\frac{\partial^2 \psi_{\mathrm{R}}}{\partial c_{\mathrm{R}}^\alpha \partial T}\,, \qquad \mu_\alpha^{\mathrm{u}} = \frac{\partial \psi_{\mathrm{R}}}{\partial c_{\mathrm{R}}^\alpha} - T\frac{\partial^2 \psi_{\mathrm{R}}}{\partial c_{\mathrm{R}}^\alpha \partial T}\,, \tag{33}$$

where the expression $\mu_\alpha = \mu_\alpha^u - T\mu_\alpha^\eta$ together with Eqs. (31),(33), is employed to determine μ_α^{u}: see Arricca et al. (2023) for a detailed derivation and discussion.

6. Helmholtz free energy and constitutive relations

Since thermal diffusivity is 10^3 to 10^4 times larger than the diffusion constant of the solvent, the rate of the heat transfer process is much higher and the simplifying hypothesis of thermal equilibrium can be adopted (Doi, 2009). Whereas the Helmholtz free energy density ψ_{R} of standard gels consists of the elasticity of the polymer network $\psi_{\mathrm{R}}^{\mathrm{el}}$ and the entropic mixing between the hosting material and the solvent $\psi_{\mathrm{R}}^{\mathrm{mix}}$, we extend it to GPEs as follows

$$\psi_{\mathrm{R}} = \psi_{\mathrm{R}}^0 + \psi_{\mathrm{R}}^{\mathrm{el}} + \psi_{\mathrm{R}}^{\mathrm{in}} + \psi_{\mathrm{R}}^{\mathrm{mix}} + \psi_{\mathrm{R}}^{\mathrm{ion-sol}} + \psi_{\mathrm{R}}^{\mathrm{pol}} + \psi_{\mathrm{R}}^{\mathrm{es}}\,, \tag{34}$$

where separate terms stand for: the standard Helmholtz free energy ψ_{R}^0; the free energy associated with the elastic deformation of the hosting material $\psi_{\mathrm{R}}^{\mathrm{el}}(\mathbf{C}, c_{\mathrm{R}}^{\mathrm{S}})$; the free energy due to the inelastic contributions $\psi_{\mathrm{R}}^{\mathrm{in}}(\mathbf{C}, \boldsymbol{\xi}_m, c_{\mathrm{R}}^{\mathrm{S}})$; the (entropic) free energy due to the interactions between the solvent and the host material $\psi_{\mathrm{R}}^{\mathrm{mix}}(c_{\mathrm{R}}^{\mathrm{S}})$; the free energy due to the interactions between the solvent and its solutes $\psi_{\mathrm{R}}^{\mathrm{ion-solv}}(c_{\mathrm{R}}^{\mathrm{S}}, c_{\mathrm{R}}^{\mathrm{Li_f^+}}, c_{\mathrm{R}}^{\mathrm{X}^-})$; the free energy due to the interactions between the species involved in the chemical reaction (1) and polymer $\psi_{\mathrm{R}}^{\mathrm{pol}}(c_{\mathrm{R}}^{\mathrm{Li_p^+}}, c_{\mathrm{R}}^{\mathrm{A}^-}, c_{\mathrm{R}}^{\mathrm{LiA}})$; the free energy due to the electro-quasi-static contribution $\psi_{\mathrm{R}}^{\mathrm{es}}(\vec{D}, \mathbf{C})$.

The standard Helmholtz free energy is defined as:

$$\psi_{\mathrm{R}}^0 = \sum_\alpha \mu_0^\alpha c_{\mathrm{R}}^\alpha, \tag{35}$$

where μ_0^α is the reference chemical potential of the α species.

In the realm of visco-elasticity, the elastic free-energy $\psi_{\mathrm{R}}^{\mathrm{el}}$ is usually further decomposed in the volumetric and isochoric contributions (Holzapfel, 2001; Simo and Hughes, 1998). We adopt a slightly compressible Neo-Hookean (hyperelastic) model (Ganser et al., 2019; Bucci et al., 2016)

$$\psi_{\mathrm{R}}^{\mathrm{el,vol}}(\mathbf{C}^{e^v}, c_{\mathrm{R}}^{\mathrm{S}}) = J_s\,\frac{\mathrm{G}}{2}\,(\mathrm{tr}\left[\,\mathbf{C}^e\,\right] - 3) \tag{36}$$
$$\psi_{\mathrm{R}}^{\mathrm{el,iso}}(\mathbf{C}^{e^i}, c_{\mathrm{R}}^{\mathrm{S}}) = J_s\,\frac{3K - 2\mathrm{G}}{6}\,(\ln\left[J_e\right])^2 - J_s\,\mathrm{G}\ln\left[J_e\right] \tag{37}$$

where K and G are the bulk and shear modulus, respectively. The inelastic counterpart has one separate expression $\psi_{\mathrm{R}}^{\mathrm{in},m}$ for each mechanisms of viscous dissipation. Eventually, the mechanical free energy $\psi_{\mathrm{R}}^{\mathrm{el}} + \psi_{\mathrm{R}}^{\mathrm{in}}$ writes as:

$$\psi_{\mathrm{R}}^{\mathrm{el,vol}}(\mathbf{C}^{e^v}, c_{\mathrm{R}}^{\mathrm{S}}) + \psi_{\mathrm{R}}^{\mathrm{el,iso}}(\mathbf{C}^{e^i}, c_{\mathrm{R}}^{\mathrm{S}}) + \sum_m \psi_{\mathrm{R}}^{\mathrm{in},m}(\mathbf{C}^e - \boldsymbol{\xi}_m, c_{\mathrm{R}}^{\mathrm{S}}). \tag{38}$$

The inelastic free energies $\psi_{\mathrm{R}}^{\mathrm{in},m}$ can be arbitrary chosen either from polymer statistical mechanics or phenomenological extrapolation (Doi, 2009), as long as the constraint

$$2\frac{\partial \psi_{\mathrm{R}}^{\mathrm{in},m}}{\partial \mathbf{C}} = -\frac{\partial \psi_{\mathrm{R}}^{\mathrm{in},m}}{\partial \boldsymbol{\xi}_m}\,, \tag{39}$$

holds (Holzapfel, 2001). Examples of $\psi_{\mathrm{R}}^{\mathrm{in},m}$ can be found in Holzapfel (2001), Bacca and McMeeking (2017), Simo and Hughes (1998), Wang and Hong (2012). On the basis of the definition (30), we deduce:

$$\boldsymbol{\Xi}_m = 2\frac{\partial \psi_{\mathrm{R}}^{\mathrm{in},m}}{\partial \mathbf{C}}\,, \qquad \mathbf{S} = 2\frac{\partial \psi_{\mathrm{R}}}{\partial \mathbf{C}} = 2\frac{\partial \psi_{\mathrm{R}}^{el}}{\partial \mathbf{C}} + 2\sum_m \frac{\partial \psi_{\mathrm{R}}^{\mathrm{in},m}}{\partial \mathbf{C}} = 2\frac{\partial \psi_{\mathrm{R}}^{el}}{\partial \mathbf{C}} + \sum_m \boldsymbol{\Xi}_m\,. \tag{40}$$

Eq. (40) connotes $\boldsymbol{\Xi}_m$ as a non-equilibrium stress tensor, uniquely identified provided that a rate equation for every internal variable $\boldsymbol{\xi}_m$ is given (Holzapfel, 2001).

The entropic mixing $\psi_{\mathrm{R}}^{\mathrm{mix}}$ between solvent and polymer network is described as in Flory (1942), Huggins (1942), Flory et al. (1943), Narayan and Anand (2022)

$$\psi_{\mathrm{R}}^{\mathrm{mix}} = \frac{\mathrm{RT}}{\Omega_{\mathrm{S}}}\left(\Omega_{\mathrm{S}} c_{\mathrm{R}}^{\mathrm{S}}\,\ln\left[\frac{\Omega_{\mathrm{S}} c_{\mathrm{R}}^{\mathrm{S}}}{1 + \Omega_{\mathrm{S}} c_{\mathrm{R}}^{\mathrm{S}}}\right] + \chi\,\frac{\Omega_{\mathrm{S}} c_{\mathrm{R}}^{\mathrm{S}}}{1 + \Omega_{\mathrm{S}} c_{\mathrm{R}}^{\mathrm{S}}}\right), \tag{41}$$

where Ω_{S} is the molar volume of the solvent. For the polymer-solvent mixing we make use of a dimensionless parameter χ which accounts for the energetic interactions between the solvent and the polymer (Narayan and Anand, 2022).

The Helmholtz free energy $\psi_{\mathrm{R}}^{\mathrm{ion-solv}}$ that depicts the interactions between solvent and ions in the mixing is written following (Narayan and Anand, 2022) as

$$\psi_{\mathrm{R}}^{\mathrm{ion-solv}} = \mathrm{RT}c_{\mathrm{R}}^{\mathrm{S}}\left[\frac{c_{\mathrm{R}}^{\mathrm{Li_f^+}}}{c_{\mathrm{R}}^{\mathrm{S}}}\,\ln\frac{c_{\mathrm{R}}^{\mathrm{Li_f^+}}}{c_{\mathrm{R}}^{\mathrm{S}}} + \frac{c_{\mathrm{R}}^{\mathrm{X}^-}}{c_{\mathrm{R}}^{\mathrm{S}}}\,\ln\frac{c_{\mathrm{R}}^{\mathrm{X}^-}}{c_{\mathrm{R}}^{\mathrm{S}}} - \frac{c_{\mathrm{R}}^{\mathrm{Li_f^+}} + c_{\mathrm{R}}^{\mathrm{X}^-}}{c_{\mathrm{R}}^{\mathrm{S}}}\right]. \tag{42}$$

The entropic Helmholtz free energy of mixing between the species involved in the polymer charge transport reaction (1) and polymer matrix $\psi_{\mathrm{R}}^{\mathrm{pol}}$ is given by Bonanno et al. (2023), Arricca et al. (2023):

$$\psi_{\mathrm{R}}^{\mathrm{pol}} = \mathrm{RT}\overline{c}_{\mathrm{R}}^\alpha\,\left[\,\theta_{\mathrm{R}}^\alpha \ln\left(\theta_{\mathrm{R}}^\alpha\right) + \left(1 - \theta_{\mathrm{R}}^\alpha\right)\ln\left(1 - \theta_{\mathrm{R}}^\alpha\right)\,\right] \quad \text{with } \alpha = \mathrm{A}^-, \mathrm{Li_p^+}, \mathrm{LiA}\,, \tag{43}$$

where $\theta_{\mathrm{R}}^\alpha = c_{\mathrm{R}}^\alpha/\overline{c}_{\mathrm{R}}^\alpha$, is the ratio of concentration c_{R}^α to the max number of ionic species hosted by the polymer network $\overline{c}_{\mathrm{R}}^\alpha$. Finally, the electrostatic Helmholtz free energy is a quadratic form $\psi_{\mathrm{es}} = |\vec{d}|^2/(2\epsilon)$ in the current configuration, hence its referential form reads (Narayan and Anand, 2022; Ganser et al., 2019)

$$\psi_{\mathrm{R}}^{\mathrm{es}} = \frac{1}{2J\epsilon}\vec{D} \cdot \mathbf{C}\vec{D}\,, \tag{44}$$

since $\vec{D}$ transforms covariantly.

Application of the thermodynamic prescriptions (31) yields

$$\vec{D} = -\epsilon J\,\mathbf{C}^{-1}\,\mathrm{Grad}\left[\,\phi\,\right]\,, \tag{45a}$$

$$\overline{\mu}_\alpha = \mu_0^\alpha + \mathrm{RT}\,\ln[\,\frac{c_\mathrm{R}^\alpha}{c_\mathrm{R}^\mathrm{S}}\,] + \mathbb{F}\,z_\alpha\,\phi, \quad \text{with } \alpha = \mathrm{Li_f^+}, \mathrm{X^-}\,, \tag{45b}$$

$$\overline{\mu}_\alpha = \mu_0^\alpha + \mathrm{RT}\,\ln[\,\frac{\theta_\mathrm{R}^\alpha}{1-\theta_\mathrm{R}^\alpha}\,] + \mathbb{F}\,z_\alpha\,\phi, \quad \text{with } \alpha = \mathrm{Li_p^+}, \mathrm{A^-}, \tag{45c}$$

$$\mu_\mathrm{LiA} = \mu_0^\mathrm{LiA} + \mathrm{RT}\ln[\,\frac{\theta_\mathrm{R}^\mathrm{LiA}}{1-\theta_\mathrm{R}^\mathrm{LiA}}\,]\,, \tag{45d}$$

$$\mu_\mathrm{S} = \mu_s^0 + \mathrm{RT}\left[\ln\frac{\Omega_\mathrm{S}c_\mathrm{R}^\mathrm{S}}{1+\Omega_\mathrm{S}c_\mathrm{R}^\mathrm{S}} + \frac{1}{1+\Omega_\mathrm{S}c_\mathrm{R}^\mathrm{S}} + \frac{\chi}{\left(1+\Omega_\mathrm{S}c_\mathrm{R}^\mathrm{S}\right)^2} - \frac{c_\mathrm{R}^{\mathrm{Li_f^+}} + c_\mathrm{R}^{\mathrm{X^-}}}{c_\mathrm{R}^\mathrm{S}}\right] + \\ +\Omega_s\left[\frac{5}{6}\,\mathrm{G}\left(\frac{\mathrm{tr}\,[\,\mathbf{C}\,]}{J_s^{2/3}} - 3\right) + \ln[J_e]\left(\frac{3K-2\mathrm{G}}{6}\,(\ln[J_e]-2) - \mathrm{G}\right)\right]\,, \tag{45e}$$

$$\mathbf{S} = \mathrm{G}\,J_s^{1/3}\,\mathbf{1} + \frac{\vec{D}\otimes\vec{D}}{\epsilon J} + \left[J_s\,\ln\left[J_e\right]\left(K-\frac{2}{3}\mathrm{G}\right) - J_s\,\mathrm{G} - \frac{\vec{D}\cdot\mathbf{C}\vec{D}}{2\epsilon J} + \psi_\mathrm{R}^\mathrm{pol}\right] \\ \mathbf{C}^{-1} + \sum_m\,\Xi_m\,. \tag{45f}$$

The mass action laws:

$$\mathrm{w}_\mathrm{R}^{(1)} = k_{f_R}^{(1)}\frac{\theta_\mathrm{R}^{\mathrm{Li_A}}}{1-\theta_\mathrm{R}^{\mathrm{Li_A}}} - k_{b_R}^{(1)}\frac{\theta_\mathrm{R}^{\mathrm{Li_p^+}}}{1-\theta_\mathrm{R}^{\mathrm{Li_p^+}}}\frac{\theta_\mathrm{R}^{\mathrm{A^-}}}{1-\theta_\mathrm{R}^{\mathrm{A^-}}}\,, \tag{46a}$$

$$\mathrm{w}_\mathrm{R}^{(2)} = k_{f_R}^{(2)}\frac{\theta_\mathrm{R}^{\mathrm{Li_p^+}}}{1-\theta_\mathrm{R}^{\mathrm{Li_p^+}}} - k_{b_R}^{(2)}\frac{c_\mathrm{R}^{\mathrm{Li_f^+}}}{c_\mathrm{R}^\mathrm{S}} \tag{46b}$$

model the kinetics of reactions (1) and (2), where $k_{f_R}^j$ and $k_{b_R}^j$ are the forward and backward reaction constants, respectively. It has been shown in Arricca et al. (2023) that the mass action law satisfies the thermodynamically constraint Eq. (32a).

To write a set of constitutive relations between the fluxes of species and their thermodynamic gradients, we adopt the Maxwell–Stefan approach, as in Narayan and Anand (2022). Alternative ways to relate fluxes to concentrations, based on a Fickian approach, are described in Arricca et al. (2023). By mapping the inequality (32b) in the current configuration

$$-\sum_\nu \mathbf{F}^{-1}\vec{h}_\nu\cdot\mathbf{F}^T\mathrm{grad}\left[\,\overline{\mu}_\nu\,\right] = -\sum_\nu\left(\vec{v}_\nu-\vec{v}_\mathrm{p}\right)\cdot\left(-c_\nu\mathrm{grad}\left[\,\overline{\mu}_\nu\,\right]\right) \geq 0 \\ \nu = \mathrm{S}, \mathrm{Li_p^+}, \mathrm{Li_f^+X^-}\,, \tag{47}$$

we can correlate the relative velocities $\left(\vec{v}_\nu-\vec{v}_\mathrm{p}\right)$ to the gradients of the electro-chemical potentials.[5] We take into account the friction forces $\mathrm{f}_{\nu\tau}$ between the components of the fluid–solid mixture in the following way

$$-c_\nu\mathrm{grad}\left[\,\overline{\mu}_\nu\,\right] = \frac{\mathrm{f}_{\nu\mathrm{p}}}{c_\nu}\vec{h}_\nu + \sum_{\alpha\neq\nu}\frac{\mathrm{f}_{\nu\alpha}}{c_\alpha c_\nu}\left(c_\alpha\vec{h}_\nu - c_\nu\vec{h}_\alpha\right)\,, \\ \alpha = \mathrm{S}, \mathrm{LiA}, \mathrm{Li_p^+}, \mathrm{A^-}, \mathrm{Li_f^+}, \mathrm{X^-}\,, \tag{48}$$

with $\mathrm{f}_{\nu\tau} = \mathrm{f}_{\tau\nu}$. Define with $\mathrm{f}_\mathrm{S} = c_\mathrm{S}\mathrm{RT}/\mathrm{f}_{\mathrm{Sp}}$ the diffusivity of the solvent, $\mathrm{f}_{\mathrm{Li_f^+}} = c_{\mathrm{Li_f^+}}\mathrm{RT}/\mathrm{f}_{\mathrm{Li_f^+S}}$, $\mathrm{f}_{\mathrm{X^-}} = c_{\mathrm{X^-}}\mathrm{RT}/\mathrm{f}_{\mathrm{X^-S}}$ the diffusivity of the solutes and polymer chain $\mathrm{f}_{\mathrm{Li_p^+}} = c_{\mathrm{Li_p^+}}\mathrm{RT}/\mathrm{f}_{\mathrm{Li_p^+p}}$ - see also (Narayan and Anand, 2022). The constitutive laws for referential fluxes descend from Eq. (48), through the pull-back operator for fluxes (see Eq. (5))

$$\vec{H}_{\mathrm{Li_p^+}} = -\frac{\mathrm{f}_{\mathrm{Li_p^+}}}{\mathrm{RT}}\,c_{\mathrm{p_R^+}}^{\mathrm{Li}}\,\mathbf{C}^{-1}\mathrm{Grad}\left[\,\overline{\mu}_{\mathrm{Li_p^+}}\,\right]\,, \tag{49a}$$

$$\vec{H}_\mathrm{S} = \frac{\mathrm{f}_\mathrm{S}}{\mathrm{RT}}\,c_\mathrm{R}^\mathrm{S}\,\mathbf{C}^{-1}\,\mathrm{Grad}\left[\,\mu_\mathrm{S}\,\right]\frac{\mathrm{f}_\mathrm{S}}{\mathrm{RT}}\,c_\mathrm{R}^\mathrm{S}\,\mathbf{C}^{-1}\left(\frac{c_{\mathrm{f_R^+}}^{\mathrm{Li}}}{c_\mathrm{R}^\mathrm{S}}\mathrm{Grad}\left[\,\overline{\mu}_{\mathrm{Li_f^+}}\,\right] + \frac{c_\mathrm{R}^{\mathrm{X^-}}}{c_\mathrm{R}^\mathrm{S}}\mathrm{Grad}\left[\,\overline{\mu}_{\mathrm{X^-}}\,\right]\right)\,, \tag{49b}$$

$$\vec{H}_{\mathrm{Li_f^+}} = -\frac{\mathrm{f}_{\mathrm{Li_f^+}}}{\mathrm{RT}}\,c_{\mathrm{f_R^+}}^{\mathrm{Li}}\,\mathbf{C}^{-1}\mathrm{Grad}\left[\,\overline{\mu}_{\mathrm{Li_f^+}}\,\right] + \frac{c_{\mathrm{f_R^+}}^{\mathrm{Li}}}{c_\mathrm{R}^\mathrm{S}}\,\vec{H}_\mathrm{S}\,, \tag{49c}$$

$$\vec{H}_{\mathrm{X^-}} = -\frac{\mathrm{f}_{\mathrm{X^-}}}{\mathrm{RT}}\,c_\mathrm{R}^{\mathrm{X^-}}\,\mathbf{C}^{-1}\mathrm{Grad}\left[\,\overline{\mu}_{\mathrm{X^-}}\,\right] + \frac{c_\mathrm{R}^{\mathrm{X^-}}}{c_\mathrm{R}^\mathrm{S}}\,\vec{H}_\mathrm{S}\,, \tag{49d}$$

As in Bacca and McMeeking (2017), we identify at least three mechanisms of viscous dissipation: the viscosity due to the transport of the fluid-mixture (solvent S and solutes $\mathrm{Li_f^+}, \mathrm{X^-}$) throughout the polymer network, the shear viscosity of the solvent itself as a viscous fluid (Wang and Hong, 2012; Bacca and McMeeking, 2017), and finally the viscoelasticity of the polymer matrix. The first dissipative phenomenon is accounted for by Maxwell–Stefan relations, which will be described later in the paper. The second type of dissipative mechanisms is representative of those viscous dissipations that occur in the GPE due to the flow of the solvent uncoupled with the one involved during its transport through the polymer matrix. This is the case for the viscous effects associated to the affine motion of the solvent with the polymer lattice (Bacca and McMeeking, 2017). The viscous behavior of the polymer network emerges due to the free polymer chains, whereas the hyperelastic response is attributed to the cross-links and entanglement of the networks (Narayanan et al., 2023; Vernerey et al., 2017). Those two mechanisms are captured by means of a linear correlation between thermodynamic fluxes and forces (Bonanno et al., 2023), in agreement with inequality (32c) and the Onsager reciprocal relation for the inelastic internal entropy production,

$$\Xi_m = \mathbf{L}_m\,\frac{d\xi_m}{dt} \qquad \forall m\,, \tag{50}$$

where $\mathbf{L}_m$ is a positive definite operator. Examples of evolution equations $\frac{d\xi_m}{dt}$ can be found in Simo and Hughes (1998).

7. Governing equations

The governing equations emerge coupling the balance equations with the constitutive specifications. They are written in terms of the state variables c_R^α, ϕ, and $\vec{U}$ in the reference configuration, i.e.,

$$\frac{d}{dt}c_R^\mathrm{S} + \mathrm{Div}\left[\,\vec{H}_S(c_\mathrm{R}^\mathrm{S}, c_\mathrm{R}^{\mathrm{Li_f^+}}, c_\mathrm{R}^{\mathrm{X^-}}, \phi, \vec{U})\,\right] = 0\,, \tag{51a}$$

$$\frac{d}{dt}c_R^{\mathrm{LiA}} + \mathrm{w}_\mathrm{R}^{(1)}(c_\mathrm{R}^{\mathrm{LiA}}, c_\mathrm{R}^{\mathrm{Li_p^+}}, c_\mathrm{R}^{\mathrm{A^-}}, \vec{U}) = 0\,, \tag{51b}$$

$$\frac{d}{dt}c_R^{\mathrm{Li_p^+}} + \mathrm{Div}\left[\,\vec{H}_{\mathrm{Li_p^+}}(c_\mathrm{R}^{\mathrm{Li_p^+}}, \phi, \vec{U})\,\right] - \mathrm{w}_\mathrm{R}^{(1)}(c_\mathrm{R}^{\mathrm{LiA}}, c_\mathrm{R}^{\mathrm{Li_p^+}}, c_\mathrm{R}^{\mathrm{A^-}}, \vec{U}) \\ + \mathrm{w}_\mathrm{R}^{(2)}(c_\mathrm{R}^\mathrm{S}, c_\mathrm{R}^{\mathrm{Li_p^+}}, c_\mathrm{R}^{\mathrm{Li_f^+}}, \vec{U}) = 0\,, \tag{51c}$$

$$\frac{d}{dt}c_R^{\mathrm{A^-}} - \mathrm{w}_\mathrm{R}^{(1)}(c_\mathrm{R}^{\mathrm{LiA}}, c_\mathrm{R}^{\mathrm{Li_p^+}}, c_\mathrm{R}^{\mathrm{A^-}}, \vec{U}) = 0\,, \tag{51d}$$

$$\frac{d}{dt}c_R^{\mathrm{X^-}} + \mathrm{Div}\left[\,\vec{H}_{\mathrm{X^-}}(c_\mathrm{R}^\mathrm{S}, c_\mathrm{R}^{\mathrm{Li_f^+}}, c_\mathrm{R}^{\mathrm{X^-}}, \phi, \vec{U})\,\right] = 0\,, \tag{51e}$$

$$\frac{d}{dt}c_R^{\mathrm{Li_f^+}} + \mathrm{Div}\left[\,\vec{H}_{\mathrm{Li_f^+}}(c_\mathrm{R}^\mathrm{S}, c_\mathrm{R}^{\mathrm{Li_f^+}}, c_\mathrm{R}^{\mathrm{X^-}}, \phi, \vec{U})\,\right] - \mathrm{w}_\mathrm{R}^{(2)}(c_\mathrm{R}^\mathrm{S}, c_\mathrm{R}^{\mathrm{Li_p^+}}, c_\mathrm{R}^{\mathrm{Li_f^+}}, \vec{U}) = 0\,, \tag{51f}$$

$$\mathrm{Div}\left[\,\mathbf{P}(c_\mathrm{R}^\mathrm{S}, c_\mathrm{R}^{\mathrm{Li_p^+}}, c_\mathrm{R}^{\mathrm{A^-}}, \phi, c_\mathrm{R}^{\mathrm{LiA}}, \vec{U}, \xi_m)\,\right] + \vec{B} = \vec{0}\,, \tag{51g}$$

$$\mathrm{Div}\left[\,\mathbb{F}\left(\vec{H}_{\mathrm{Li_p^+}}(c_\mathrm{R}^{\mathrm{Li_p^+}}, \phi, \vec{U}) + \vec{H}_{\mathrm{Li_f^+}}(c_\mathrm{R}^\mathrm{S}, c_\mathrm{R}^{\mathrm{Li_f^+}}, \phi, \vec{U}) - \vec{H}_{\mathrm{X^-}}(c_\mathrm{R}^\mathrm{S}, c_\mathrm{R}^{\mathrm{X^-}}, \phi, \vec{U})\right) + \frac{d}{dt}\vec{D}(\phi, \vec{U})\,\right] = 0. \tag{51h}$$

Neumann boundary conditions

$$\mathbf{P}\,\vec{N} = \vec{\bar{t}} \qquad \vec{X}\in\partial^N\Omega_\mathrm{R}\,, \quad \vec{H}_\alpha\cdot\vec{N} = \overline{H}_\alpha \qquad \vec{X}\in\partial^N\Omega_\mathrm{R}\,, \\ \vec{I}\cdot\vec{N} = \overline{I} \qquad \vec{X}\in\partial^N\Omega_\mathrm{R}\,, \tag{52}$$

are imposed along the boundaries $\partial^N\Omega_\mathrm{R}$. Dirichlet boundary conditions shall be imposed along the complementary boundary $\partial^D\Omega_\mathrm{R}$,

$$\vec{U} = \overline{\vec{U}} \qquad \vec{X}\in\partial^D\Omega_\mathrm{R}\,, \qquad \phi = \overline{\phi} \qquad \vec{X}\in\partial^D\Omega_\mathrm{R}\,, \tag{53}$$

[5] We neglect the frictional forces exchanged by solutes dissolved in the solvent with the host polymer network as well as the frictional forces interchanged among the solutes. Hence, we consider only the frictional forces between the solvent and the solid polymer f_{PS}, the solvent and the solutes $f_{\mathrm{Li_f^+S}}$, $f_{\mathrm{X^-S}}$, and between the species $\mathrm{Li_p^+}$ and the solid polymer network $f_{\mathrm{PLi_p^+}}$.

Table 3
Model parameters used for numerical simulations.

Input parameters				
Parameters	Values	Units	Description	References
T	298.15	K	Temperature	[*this work*]
L_e	$5.00 \cdot 10^{-4}$	m	Thickness of the GPE	Jabbari et al. (2022)
A	$1.00 \cdot 10^{-4}$	m^2	Geometrical surface area	[*this work*]
$\not{d}_{\mathrm{Li}_p^+}$	$2.00 \cdot 10^{-14}$	m^2/s	Diffusion coefficient for Li_p^+ ions	[*this work*]
$\not{d}_{\mathrm{Li}_f^+}$	$2.00 \cdot 10^{-11}$	m^2/s	Diffusion coefficient for Li_f^+ ions	Danilov and Notten (2008)
$\not{d}_{\mathrm{X}^-}$	$3.00 \cdot 10^{-11}$	m^2/s	Diffusion coefficient for X^- ions	Danilov and Notten (2008)
$\not{d}_{\mathrm{S}}$	$5.00 \cdot 10^{-9}$	m^2/s	Diffusion coefficient for the solvent	Chester and Anand (2010)
$\tilde{k}^1_{f_R}$	$1.00 \cdot 10^{-4}$	$\mathrm{m}^3/(\mathrm{mol\ s})$	forward reaction constant of (1)	[*this work*]
$\tilde{k}^1_{b_R}$	$1.00 \cdot 10^{-6}$	$\mathrm{m}^3/(\mathrm{mol\ s})$	backward reaction constant of (1)	[*this work*]
$\tilde{k}^2_{f_R}$	$1.00 \cdot 10^{-5}$	$\mathrm{m}^3/(\mathrm{mol\ s})$	forward reaction constant of (2)	[*this work*]
$\tilde{k}^2_{b_R}$	$1.00 \cdot 10^{-6}$	$\mathrm{m}^3/(\mathrm{mol\ s})$	backward reaction constant of (2)	[*this work*]
G	64.00	MPa	Shear modulus	Song et al. (2017)
K	2112	MPa	Bulk modulus	Song et al. (2017)
Ω_s	$18.0 \cdot 10^{-6}$	$\mathrm{m}^3/\mathrm{mol}$	Molar volume of the solvent	Narayan and Anand (2022)
Ω_{Li}	$13.0 \cdot 10^{-6}$	$\mathrm{m}^3/\mathrm{mol}$	Molar volume of the lithium	Han et al. (2021)
χ	0.1	–	Flory–Huggins parameter	Chester and Anand (2010)
ϵ_r	4	–	Relative permittivity	Shi et al. (2018)

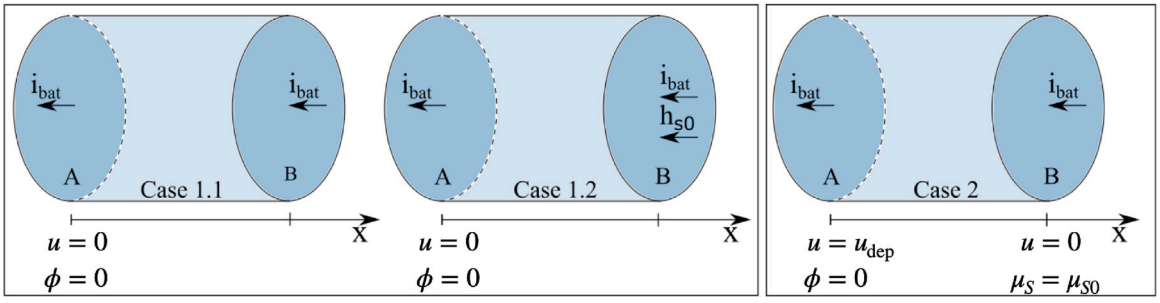

Fig. 1. Case studies of a GPE under an applied current density $i_{bat}(t)$. Case study 1 (free expansion): face A is fully restrained $\vec{U} = \vec{0}$ and face B is free to expand. Case 1.1 assumes no flux of solvent, while Case 1.2 accounts for an injection of solvent $h_{s0}(t)$ at face B. In case study 2 the face B is fully restrained $\vec{U} = \vec{0}$, whereas displacements $\vec{U}(0,t) = \vec{u}_{dep}(t)$ are imposed at face A by lithium deposition.

in order to guarantee the solvability of the set of Eqs. (51). Finally, initial conditions for the electric potential $\phi(\vec{X}, t = 0)$ and the concentrations $c^{\alpha}_{\mathrm{R}}(\vec{X}, t = 0)$, and $\xi_m(\vec{X}, t = 0)$ have to be provided.

8. Numerical simulations

A one dimensional model problem has been investigated numerically, to highlight the main features of the GPE in operating conditions of galvanostatic charge with current density $i_{bat}(t)$ at a constant temperature of 25°C. Material properties are assumed to be homogeneous, with the material free to expand laterally along the y- and z-directions and impermeable along the curved lateral surface of the cylinder shown in Fig. 1. This assumption captures the predominant deformation and transport behavior along the main axis while neglecting minor transverse gradients. Two one-dimensional[6] case studies will show the interactions between the physical quantities at stake in the electrolyte. The first study concerns a GPE which is free to expand: charge is studied in two sub-cases, either with or without mass flux of solvent at the boundary. The second study mimics the response of the GPE induced by a constrained plating, as described in Cabras and Serpelloni (2025).

Fig. 1 shows a realistic geometrical configuration of a Lithium button battery with gel polymer electrolyte. It depicts a $L_e = 5.0 \times 10^{-4}$ m thick GPE, as in Jabbari et al. (2022), with area $A = 10^{-4}$ m^2.

Material parameters have been collected in Table 3. Although a full sensitivity analysis is beyond the scope of the present study, it should be noted that several parameters – currently lacking experimental validation – may significantly influence the model response. The following virtual experiments are therefore intended to explore the model behavior using representative values of these material parameters. The diffusivity[7] of the lithium across the polymer $\not{d}_{\mathrm{Li}_p^+} = 2.00 \times 10^{-14}$ m^2/s is much smaller than the diffusivities $\not{d}_{\mathrm{Li}_f^+} = 2.10 \times 10^{-11}$ m^2/s and $\not{d}_{\mathrm{x}^-} = 3.00 \times 10^{-11}$ m^2/s in the solvent (Danilov and Notten, 2008). The diffusivity of the solvent with respect to the polymer network is taken as $\not{d}_{\mathrm{S}} = 5.00 \times 10^{-9}$ m^2/s, as in Chester and Anand (2010). We neglect the shear viscosity of the solvent and the viscoelastic contribution given by the solid polymer lattice, therefore $\boldsymbol{\Xi}_m = \mathbf{0}$. We also considered the entropic Helmholtz free energy of mixing $\psi^{\mathrm{pol}}_{\mathrm{R}}$ as secondary. The mechanical properties of the polymeric gel are defined by a shear modulus $G = 64$ MPa and a bulk modulus $K = 2112$ MPa, corresponding to an isotropic material with a Poisson ratio $\nu = 0.485$ as in Song et al. (2017). The equilibrium constants of chemical reactions (1) and (2) are taken as $K^1_{\mathrm{eq}} = 100$ and $K^2_{\mathrm{eq}} = 10$. All material parameters used in the simulations are listed in Table 3, with the related references.

Faces A and B have been named according to Fig. 1. We denote Dirichlet and Neumann boundaries with the apex D or N, and faces as subscript, such as $\partial^D_A\Omega_{\mathrm{R}}$, $\partial^N_A\Omega_{\mathrm{R}}$, $\partial^D_B\Omega_{\mathrm{R}}$ and $\partial^N_B\Omega_{\mathrm{R}}$. The flow of lithium ions across the electrode/electrolyte interfaces occurs in the polymer as well as in the liquid. The flux at the electrolyte boundary shall thus

[6] The governing equations have been specialized to the one dimensional case in Supplementary Material, *Section 2.1. 1D Problem.*

[7] In the absence of devoted experimental investigations, the Maxwell–Stefan diffusivities have been taken as constants, i.e., we assumed arbitrarily that the frictional forces are proportional to the concentrations.

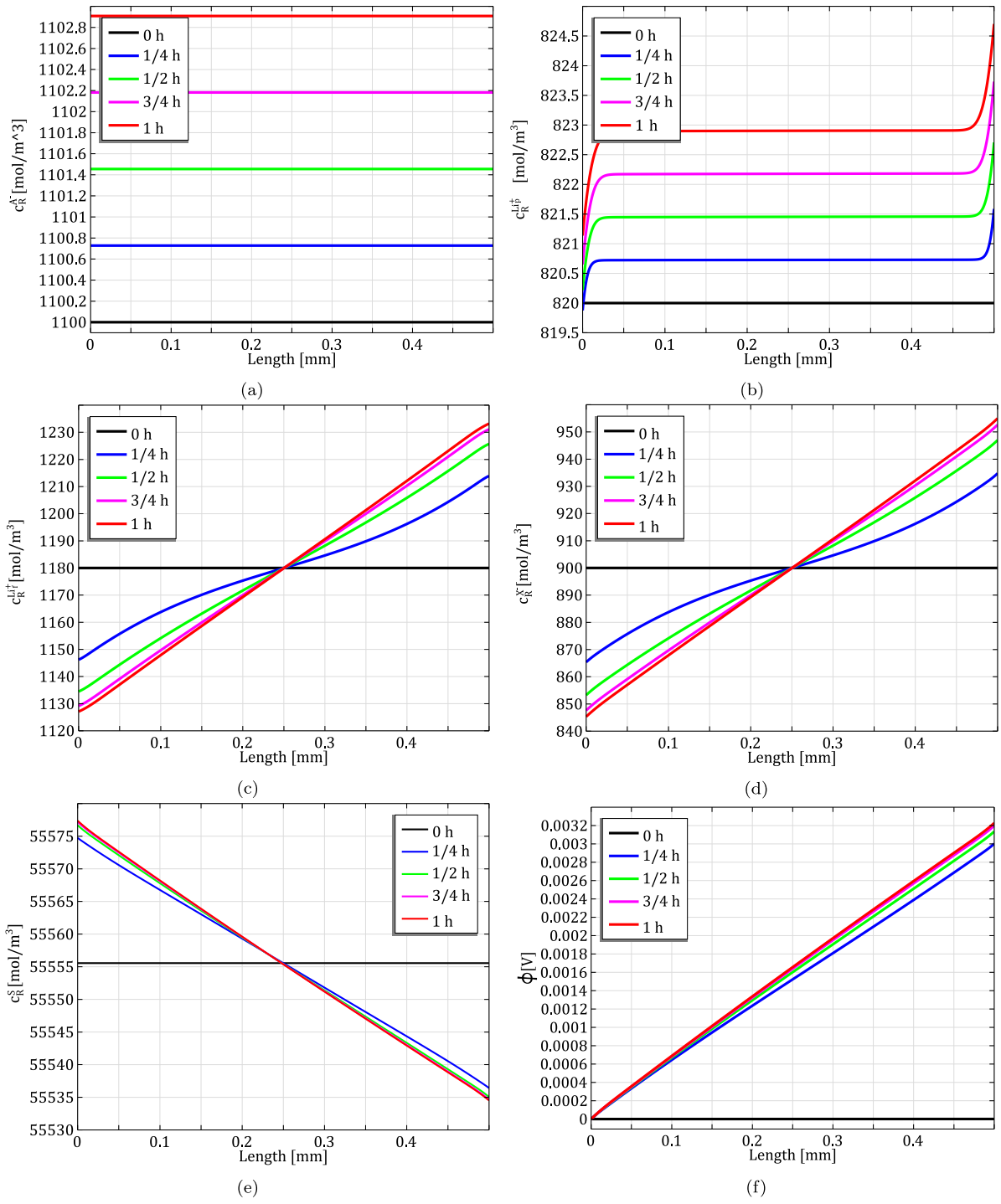

Fig. 2. Case 1.1: lithium concentration profiles of the different species $c_R^{A^-}$, $c_R^{Li_p^+}$, $c_R^{Li_f^+}$, $c_R^{X^-}$ (a)–(d), c_R^S, and of the electric potential ϕ (f), for five different time steps. The concentration sum $c_R^{LiA} + c_R^{A^-} = 10^4$ moles/m^3.

be split into two terms,

$$\vec{H}_{Li_p^+}(0,t)\cdot\vec{N} = h^{BV}_{Li_p^+}\,, \qquad \vec{H}_{Li_f^+}(0,t)\cdot\vec{N} = h^{BV}_{Li_f^+} \qquad \vec{X}\in\partial^N_A\Omega_R\,, \tag{54a}$$

$$\vec{H}_{Li_p^+}(L_e,t)\cdot\vec{N} = -h^{BV}_{Li_p^+}\,, \qquad \vec{H}_{Li_f^+}(L_e,t)\cdot\vec{N} = -h^{BV}_{Li_f^+} \qquad \vec{X}\in\partial^N_B\Omega_R. \tag{54b}$$

In modeling a whole battery cell, the mass fluxes $h^{BV}_{Li_p^+}$ and $h^{BV}_{Li_f^+}$, descend from Butler-Volmer interface equations (Dreyer et al., 2016). Here, we consider them as given quantities that satisfy the constraint

$$\mathbb{F}\left(h^{BV}_{Li_p^+} + h^{BV}_{Li_f^+}\right)\cdot\vec{N} = i_{bat}(t)\,, \quad \vec{X}\in\partial^N V, \tag{55}$$

where

$$i_{bat}(t) = (1-e^{-0.05t})\,\bar{i}_{bat}$$

is the applied charge current density, which is tuned to make boundary and initial conditions compatible. $\bar{i}_{bat}$ is the asymptotic value of the applied current density. Negative ions X^- cannot leave the electrolyte,

i.e.,

$$\vec{H}_{X^-} \cdot \vec{N} = 0, \qquad \vec{X} \in \partial^N \Omega_R.$$

The flux of solvent at $X = L_e$ is generically specified by

$$\vec{H}_S(L_e, t) \cdot \vec{N} = -(1 - e^{-0.05t})\, \bar{h}_{s_0}\,, \qquad \vec{X} \in \partial_B^N \Omega_R\,, \tag{56}$$

with $\bar{h}_{s_0}$ the maximum value of the external solvent flux. The amount of $\bar{h}_{s_0}$ will be defined separately for each case study, as depicted in Fig. 1. Since the solvent is not allowed to permeate the anode,

$$\vec{H}_S(0, t) \cdot \vec{N} = 0.$$

The concentrations of ions and of the solvent across the electrolyte at $t = 0\ s$ are uniform at equilibrium, and their initial values are:

$$\begin{aligned}
&c_R^S(X,0) = 55556\ \text{mol/m}^3 \quad c_R^{LiA}(X,0) = 8900\ \text{mol/m}^3 \qquad 0 \le X \le L_e,\\
&c_R^{A^-}(X,0) = 1100\ \text{mol/m}^3 \quad c_R^{Li_p^+}(X,0) = 820\ \text{mol/m}^3 \qquad 0 \le X \le L_e,\\
&c_R^{Li_f^+}(X,0) = 1180\ \text{mol/m}^3 \quad c_R^{X^-}(X,0) = 900\ \text{mol/m}^3 \qquad 0 \le X \le L_e.
\end{aligned} \tag{57}$$

The molar volume of the solvent, is taken form Narayan and Anand (2022) as $\Omega_S = 18 \cdot 10^{-6}\ [m^3/mol]$ and the initial volume of the solvent was assumed to be the 50% of the total volume of the gel. Consistently, the initial concentration of solvent has been estimated at $c_R^S = 55556\ [mol/m^3]$.

Boundary conditions on the Maxwell equations are imposed in the form $\frac{d\vec{D}}{dt} \cdot \vec{N} = 0$. To be consistent with initial conditions and to respect the thermodynamic equilibrium when no current flows, the electric potential at initial time has to be homogeneous $\phi(\vec{X}, 0) = 0$, $\vec{X} \in \Omega_R$ and its value at face A, imagined as the interface with a reference electrode, has been fixed to:

$$\phi(0, t) = 0 \quad \forall t \quad \text{and} \quad \vec{X} \in \partial_A^D \Omega_R. \tag{58}$$

The analytical model is implemented in COMSOL Multiphysics, using the Mathematics > PDE Interfaces, which allows solving partial differential equations (PDEs) in their most general form. Lagrange-type shape functions were employed for spatial discretizations. The domain was discretized using a regular mesh with a step size of 0.01 mm, halved in the two terminal regions (0.1 mm) to better capture the concentration gradients. A Time Dependent study was conducted to describe the temporal evolution of the field variables, with a time step of 0.1 s. The resulting linear system was solved using a Direct Solver, specifically the MUMPS (Multifrontal Massively Parallel Sparse Direct Solver). The Fully Coupled approach was applied for the solution of the coupled system.

8.1. Case study 1: free expansion

In the first case study, we analyze the 1D free expansion of a GPE in operating conditions, setting the asymptotic current density to $\bar{i}_{bat} = 1.0\ [A/m^2]$. Two instances are investigated: Case 1.1 assumes no flux of solvent, while Case 1.2 accounts for an injection of solvent $h_{s0}(t)$ at face B.

Face A, at $X = 0$, is considered as the anode/electrolyte interface. There, the electric potential ϕ has been fixed to zero, displacements are prevented $u(0, t) = 0$, and no flow of solvent is allowed. At the other end of the electrolyte, at $X = L_e$, face B represents the electrolyte/cathode interface, where displacements are free. Tractions at the boundary

$$\mathbf{P}(\vec{X}, t) \cdot \vec{N} = \vec{0}\,, \qquad \vec{X} \in \partial_B^N \Omega_R$$

vanish to allow free expansion.

Case 1.1

The profiles of concentrations $c_R^{A^-}$, $c_R^{Li_p^+}$, $c_R^{Li_f^+}$, $c_R^{X^-}$, c_R^S, and of the electric potential ϕ have been depicted in Fig. 2 at five different time steps, spanning the total time of one hour. The concentration of c_R^{LiA} can be straightforwardly obtained, since the sum $c_R^{LiA} + c_R^{A^-}$ is a constant, which equals the initial referential concentration $c_0 = 10^4$ moles/m^3 of non-dissociated LiA.

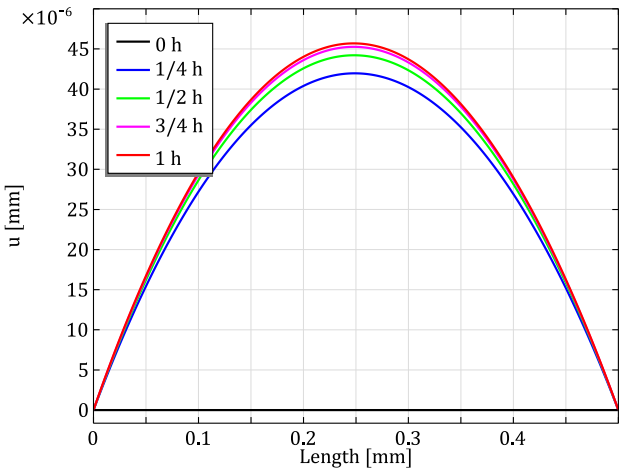

Fig. 3. Displacement profile for five time steps of Case 1.1 (no flux allowed from the interfaces).

Owing to reaction (1), a production of $c_R^{Li_p^+}$ and $c_R^{A^-}$ at the expense of c_R^{LiA} is observed, as confirmed in Fig. 2a. At the initial time, the equilibrium concentrations (57) show that the selected equilibrium constant $\tilde{K}_{eq}^{(2)}$ allow reaction (2) to occur vigorously, moving a significant amount of lithium ions (about 280 moles/m^3) from the polymer to the fluid without altering the overall electroneutrality, since $c_R^{Li_p^+} + c_R^{Li_f^+} - c_R^{A^-} - c_R^{X^-} = 0$. The increment of $c_R^{Li_f^+}$ favors the conduction and hence the battery performances, since ionic transport mostly occurs in the liquid phase, because $\phi_{Li_p^+} \ll \phi_{Li_f^+}$.

Based on Eq. (8b) and (8c), neither LiA nor A^- can flow and their concentrations are dictated merely by the rate of reaction (1). Fig. 2 manifests that reaction (1) is not boosted by the ionic redistribution during charge/discharge, since the fluctuation of c_R^{LiA} and $c_R^{A^-}$ is minimal: according to Fig. 2a only 3 moles/m^3, corresponding to less than 0.3% for $c_R^{A^-}$. Furthermore, the uniform distribution of $c_R^{A^-}$ shows that reaction (1) is not particularly influenced by gradients of $c_R^{Li_f^+}$, which are balanced by a corresponding redistribution of $c_R^{X^-}$: this event seems to show that ionic transport is poorly influenced by reaction (2) kinetics. Indeed, the concentration profile of Li_f^+ after 1 h is almost linear as in pure liquid electrolytes (Salvadori et al., 2015c), see Fig. 2(d).

The polymer phase show a concentration gradient for Li_p^+ near the ends of the electrolyte. It seems logic to attribute those gradients to a local effect of Neumann boundary conditions (54) that rapidly vanishes affecting $c_R^{A^-}$ with similar trends but with negligible amount. The resulting uniform distribution of $c_R^{A^-}$ reminds to solid polymer electrolytes (Cabras et al., 2022; Yildiz et al., 2024).

It is worth emphasizing that the total amount of solvent is conserved in Case 1.1. The solvent concentration c_R^S is influenced by the applied current, the latter being the unique effect that is macroscopically observable. Fig. 2(e) shows a reorganization of solvent inside the electrolyte. The flow of lithium ions from the right to the left determines an increment of c_R^S in the left half of the electrolyte and a reduction in the right half.

Because of Maxwell–Stefan's thermodynamics and the electro-mechanical coupling, solvent concentration, strains, and stresses are strongly interconnected. The reorganization of the solvent promotes displacements, although at a nanometric scale, in the polymer network, as shown in Fig. 3. Whereas the size of the separator remains unaltered, an

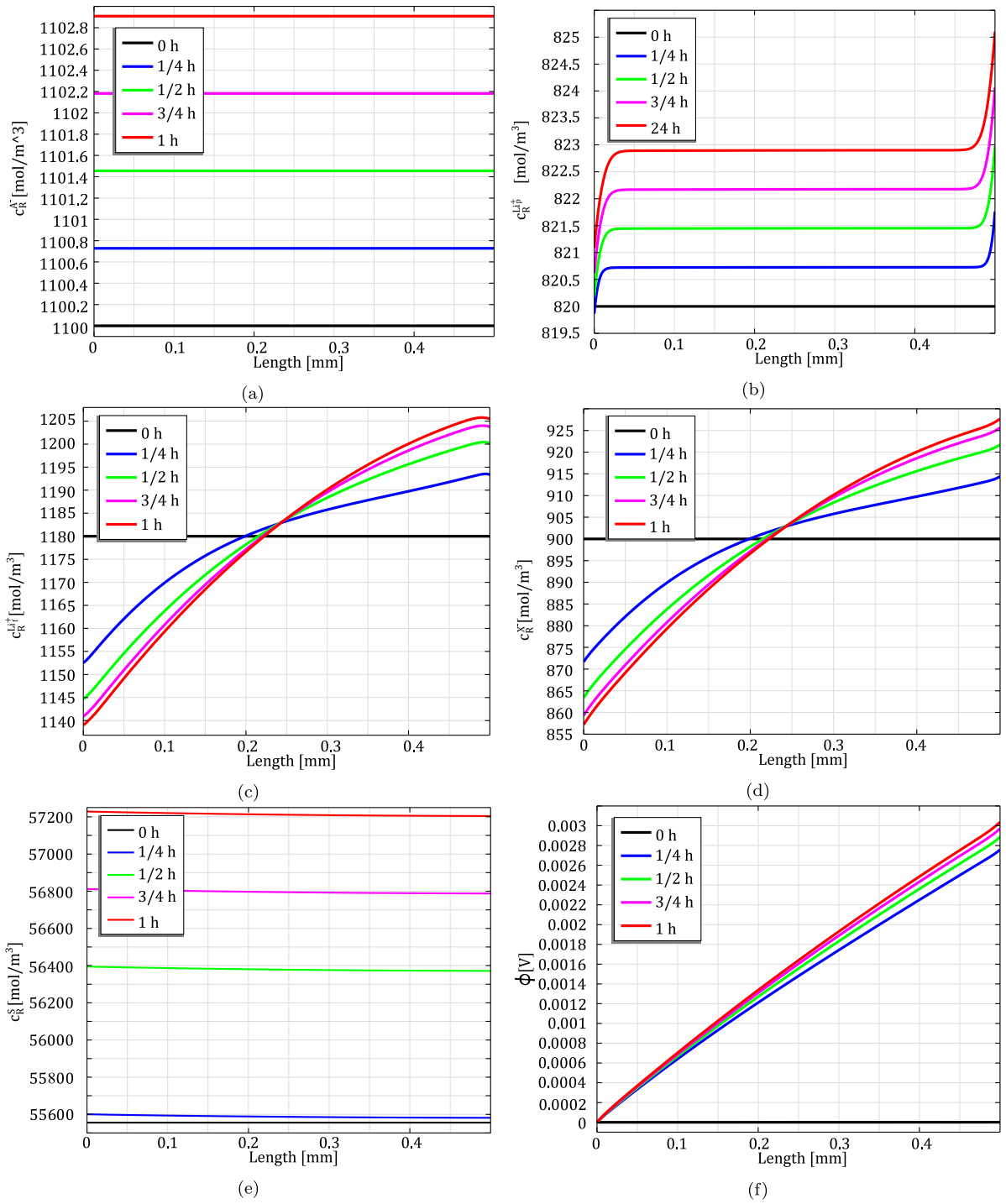

Fig. 4. Case 1.2: lithium concentration profiles of the different species $c_R^{A^-}$, $c_R^{Li_p^+}$, $c_R^{Li_f^+}$, $c_R^{X^-}$ (a)–(d), c_R^S, and of the electric potential ϕ (f), for five different time steps. The concentration sum $c_R^{LiA} + c_R^{A^-} = 10^4$ moles/m^3.

elongation in the left side of the domain is compensated by a shrinking on the right. Mechanical deformations are induced by the applied current, whereby the electrolyte is stress free and it freely expands. Fig. 2(f) plots the electric potential ϕ, which shows an almost linear trend over time.

Case 1.2

The aim of this section is studying the effect of an inward flux of solvent at $X = L_e$

$$\vec{H}_S \cdot \vec{N} = -(1 - e^{-0.05t})\, 2.31 \cdot 10^{-4}\ [\mathrm{mol}/(\mathrm{m}^2\mathrm{s})]\,, \tag{59}$$

which adds about the 3% of the initial electrolyte content in the simulation time span. Outcomes in Fig. 4 show that the general trend of the concentration profiles of all the species involved in the electrochemical process does not differ from the Case 1.1. A comparison of the plots of $c_R^{Li^+} = c_R^{Li_p^+} + c_R^{Li_f^+}$ for the two case studies is provided in Fig. 5 at five different time steps. At the injection interface (face B) a reduction of $c_R^{Li_f^+}$ and consequently of $c_R^{Li^+}$ compared to Case 1.1 occurs. At the opposite side (face A) a slight increment in $c_R^{Li^+}$ is detected.

The concentration of the solvent c_R^S is plotted in Fig. 4(e), at five different time steps. Compared with Fig. 2(e), similarities and differences

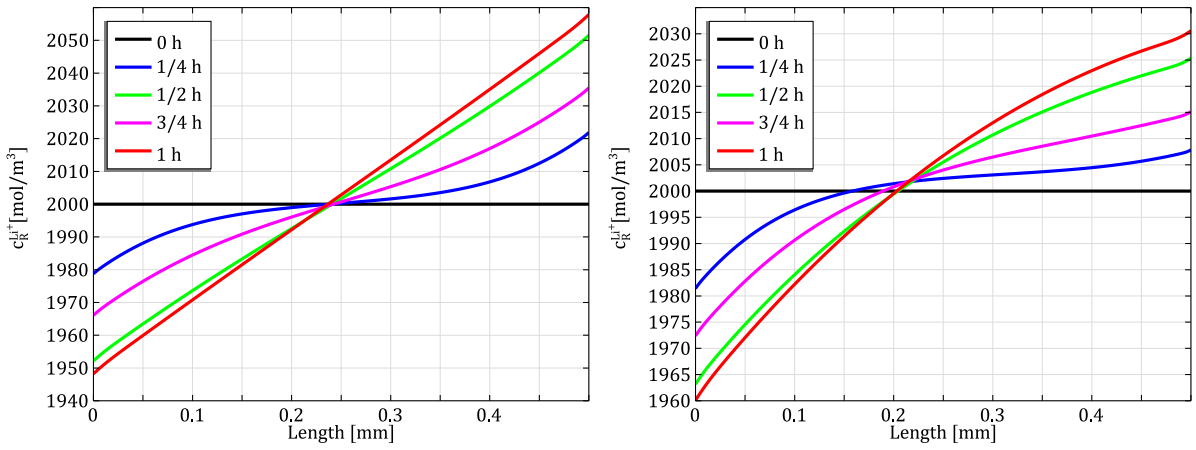

(a) Case study 1.1 (b) Case study 1.2

Fig. 5. Comparison of concentration profiles of $c_R^{\mathrm{Li}^+} = c_R^{\mathrm{Li}^+}_p + c_R^{\mathrm{Li}^+}_f$ at five different time steps. To the left, Case study 1.1, whereas Case study 1.2 is plot to the right.

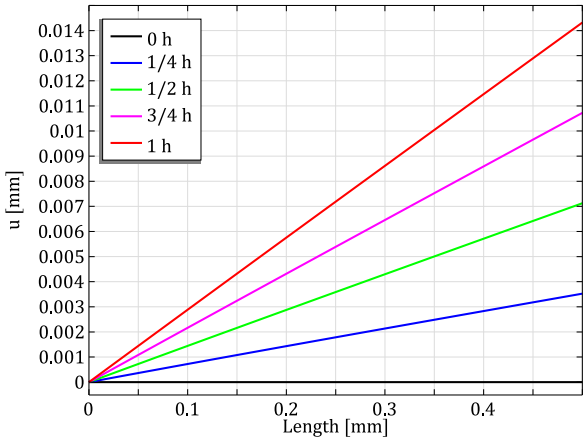

Fig. 6. Profile of the displacement u at five time steps.

emerge. As in Fig. 2(e), the external current induces a reorganization of the solvent driven by the electrochemical potentials of the ionic species, see Eq. (49b), which intensifies to the left to the detriment of the right. To such a molecular motion, which is rapid since ϕ_s is high and preserves the global mass, sums up the effect of the incoming flux in (56) which, in the absence of a ionic motion, would accumulate nearby the injection side at $X = L_e$. Since this effect is not observed, we might argue that the presence of the current causes a counter-intuitive profile of the solvent concentration c_R^S. In fact, a classical behavior with the highest concentrations nearby to the injection area, comes out when the current is turned off.

The build up of solvent mass is responsible of the swelling of the electrolyte, with consequent expansion of the polymer network, as shown in Fig. 6. The elongation of $\simeq 14.5$ μm corresponds to the $\simeq 3\%$ of the initial length of the gel.

8.2. Case study 2: "plating"

In the present case study we mimic the response of the GPE to a constrained deposition of lithium at the interface with a metal foil anode, located at the Face A in Fig. 1, having prevented displacements at Face B, i.e., $u(L_e, t) = 0$ - see also Fig. 1. The deposition takes place at a rate (Liu and Lu, 2017)

$$v_{dep}(t) = \frac{\Omega_{Li} i_{bat}(t)}{\mathbb{F}}\,, \tag{60}$$

and induces a compressive stress inside the GPE. As for the case study 1, face A is impermeable to solvent. At face B, rather than imposing a given flux of solvent as in case study 1.2, we impose a boundary condition on the chemical potential of the solvent, which is forced to remain fixed at $\mu_S(L_e, t) = -510$ J/mol throughout the simulation. Provided that, all contributions that concur to define μ_S in Eq. (45e) are free to change. Accordingly, the solvent may flow across face B.

The electro-chemical response of the GPE in this case study is conceptually similar to the case study 1. Therefore we are not indulging in further discussions on it. The evolution in time of the chemical potential of the solvent is provided in Fig. 7(a). Starting from the initial value $\mu_S(X, 0) = -510$ J/mol, μ_S increases everywhere in the GPE but at the constrained location $X = L_e$. Eventually, its profile tends to become linear because of the ions relocation and pressure rise. According to Maxwell–Stefan constitutive laws (49), a gradient in μ_S promotes the flow of solvent (Fig. 7(b)) and ions, as well as a consequent alteration of all concentration fields.

Most interesting is the mechanical response. At the end of the simulation, at $t_f = 1$ h, the constrained lithium deposition shortens the polymer electrolyte about $\simeq 0.13\%$ of its initial length. Accordingly, strains arise in the GPE, as shown in Fig. 8a. In turn, strains induce a uniform stress profile inside the GPE. The evolution in time of the first Piola stress P_{11} at a generic location is plotted in Fig. 8b.

Driven by the constrained plating with the consequent "squeezing" of the polymer, the solvent flows – see Fig. 7(b) – out of the GPE at $X = L_e$, lessening the mass of the solvent. In the absence of ionic current, see Supplementary Material - *Section 2.2. Numerical simulation - standard Gel behavior*, this phenomenon occurs generating small gradients in the solvent concentration, see Fig. 9(a). The applied current affects the trend of the solvent profile, though, inverting the flux of solvent in proximity of face A. In fact, as for the first case study, an increment of c_R^S at face A is clearly visible after 15 min, accompanied by stronger gradients, see Fig. 9(b). The solvent concentration gradually and uniformly decreases afterwards, as the solvent extraction proceeds. Intriguingly, despite the different trends in these two cases, the total amount of solvent extracted from the GPE remains comparable.

9. Conclusions

In this note we detailed a multi-scale compatible three-dimensional model of a GPE, framed in the realm of modern continuum mechanics and thermodynamics. The interplay of a fluid mixture (solvent and solutes) with a polymer solid network has been analyzed, evaluating the interactions between the lithium ions moving across the solid network

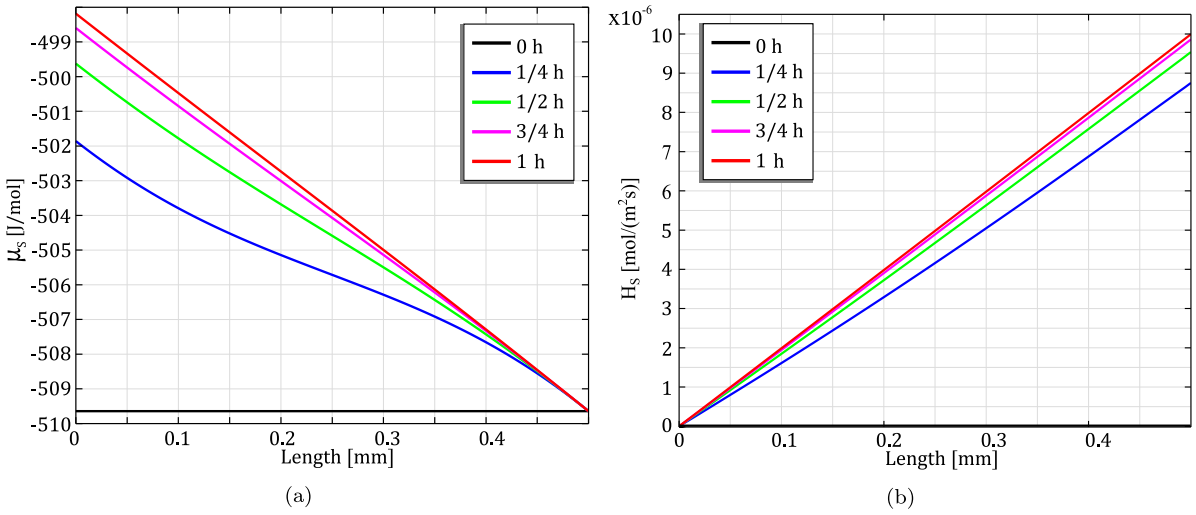

Fig. 7. (a) Profile of the electro-chemical potential of the solvent μ_S. (b) Profile of the flux of solvent H_S.

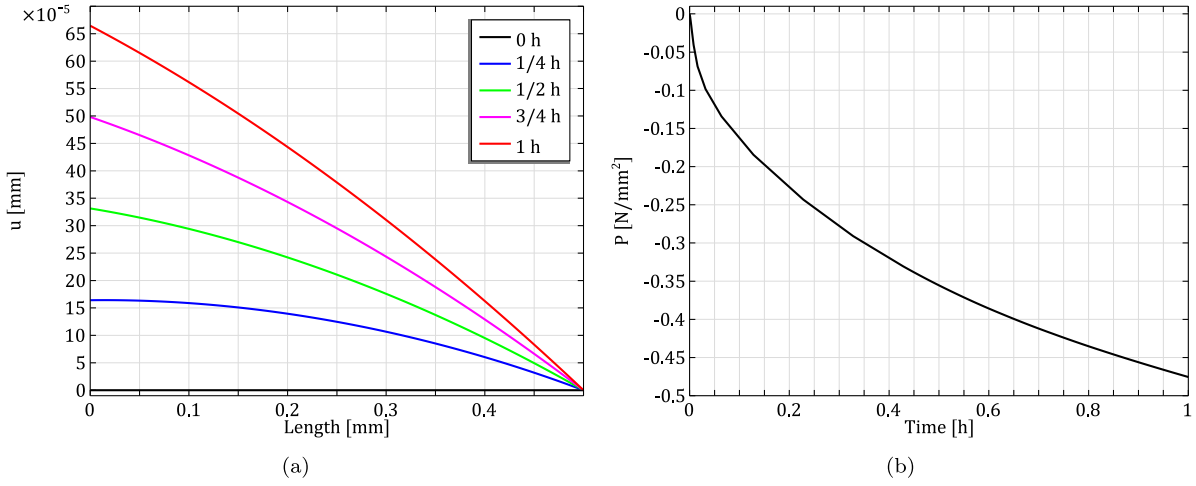

Fig. 8. (a) Displacement field profile inside the electrolyte at five different time steps. (b) Uniform first Piola stress P_{11} inside the electrolyte as a function of time.

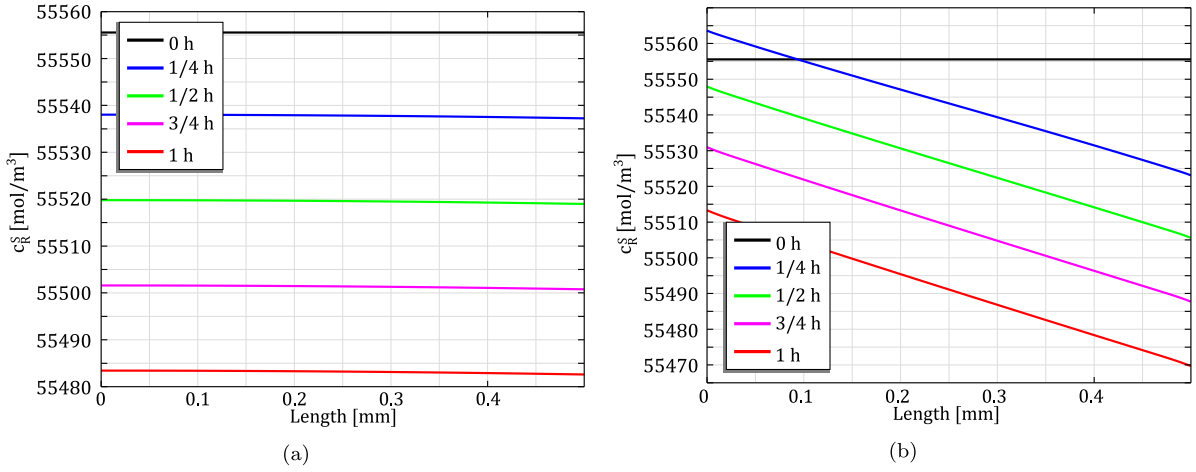

Fig. 9. Profile of the solvent concentration c_R^S, for five different time steps without (a) and with (b) flow of current.

and through the liquid phase of the gel, as well as the mechanical interactions between the solvent and the polymer network. From a mechanical standpoint, all three main mechanisms that characterize a gel have been accounted for: swelling (or drying), squeezing, and forced permeation. We emphasized the full coupling between the large deformations affecting the GPE and the transport of solvent and ions

into the gel, proposing a complex transport mechanism for the lithium ions in both polymeric and liquid phases.

The numerical approximation of the governing equations have been carried out using the COMSOL Multiphysics Finite Element Software, through the "PDE Interface" module which allows specifying the governing Eqs. (51) in strong form. We analyzed two case studies that mimic the behavior of a GPE during charge of a battery cell. The concentration profiles, the electric potential, and the displacement fields have been discussed. We have investigated the model using representative values of the material parameters, but a systematic study of parameter sensitivity is left for future work. The model captures the effect of the current on the solutes and on the solvent in agreement with the Maxwell–Stefan equations. Counter-intuitive behaviors of the GPE have been detailed in different operative conditions.

We have accounted for experimental investigations (Ford et al., 2020) on the effect of solvent in GPEs, capturing by means of Eq. (2) the increment in Li^+ mobility upon decreasing of Li^+-polymer interactions and gel solvent-polymer interactions. To the best of our knowledge, experimental data on most of the multiphysics features implemented in our work are not yet available. The theoretical and numerical findings of the paper fueled profound speculations, which may guide further experimental campaigns on GPE battery cells.

The temperature dependence in the constitutive prescriptions derived in Section 5.4 will be considered in further publications. Indeed, the assumption of thermal equilibrium prevents the description of several processes that affect the response of the GPEs.

CRediT authorship contribution statement

Mattia Serpelloni: Writing – review & editing, Writing – original draft, Visualization, Validation, Supervision, Software, Resources, Project administration, Methodology, Investigation, Formal analysis, Data curation, Conceptualization. **Alberto Salvadori:** Writing – review & editing, Visualization, Validation, Supervision, Software, Resources, Project administration, Methodology, Investigation, Funding acquisition, Formal analysis, Data curation, Conceptualization. **Luigi Cabras:** Writing – review & editing, Writing – original draft, Visualization, Validation, Supervision, Software, Resources, Project administration, Methodology, Investigation, Formal analysis, Data curation, Conceptualization.

Declaration of competing interest

The authors declare that they have no known competing financial interests or personal relationships that could have appeared to influence the work reported in this paper.

Acknowledgments

Authors are gratefully indebted with Prof. Jennifer L. Schaefer, University of Notre Dame, for the illuminating discussions on the chemistry of GPEs and bibliographical references. Authors ackwnowledge the fundings from BMW group through the project "TIMECLiP" as well as from Dassault Systemes Simulia Corp. under a devoted research collaboration agreement. This work has been partially financed by the Research Fund for the Italian Electrical System under the Three-Year Research Plan 2022–2024 (DM MITE n. 337, 15.09.2022), in compliance with the Decree of April 16th, 2018. The work has been carried out as part of INdAM (Istituto Nazionale di Alta Matematica) GNFM activities.

Appendix A. Supplementary data

Supplementary material related to this article can be found online at https://doi.org/10.1016/j.euromechsol.2025.105988.

Data availability

Data will be made available on request.

References

Anand, L., 2011. A thermo-mechanically-coupled theory accounting for hydrogen diffusion and large elastic-viscoplastic deformations of metals. Int. J. Solids Struct. 48, 962–971.

Arricca, M., Cabras, L., Serpelloni, M., Bonanno, C., McMeeking, R.M., Salvadori, A., 2023. A coupled model of transport-reaction-mechanics with trapping, Part II: Large strain analysis. J. Mech. Phys. Solids 181, 105425.

Bacca, M., McMeeking, R.M., 2017. A viscoelastic constitutive law for hydrogels. Meccanica 52 (14), 3345–3355.

Balo, L., Shalu, Gupta, H., Kumar Singh, V., Kumar Singh, R., 2017. Flexible gel polymer electrolyte based on ionic liquid emimtfsi for rechargeable battery application. Electrochim. Acta 230, 123–131.

Baskoro, Febri, Wong, Hui Qi, Yen, Hung-Ju, 2019. Strategic structural design of a gel polymer electrolyte towards a high efficiency lithium-ion battery. ACS Appl. En Mater. 2 (6), 3937–3971.

Bonanno, C., Serpelloni, M., Arricca, M., McMeeking, R.M., Salvadori, A., 2023. Actin based motility unveiled: How chemical energy is converted into motion. J. Mech. Phys. Solids 175, 105273.

Borodin, O., Smith, G.D., 2006. Mechanism of ion transport in amorphous poly(ethylene oxide)/LiTFSI from molecular dynamics simulations. Macromoleculs 39 (4), 1620–1629.

Bucci, G., Chiang, Y.-M., Carter, W.C., 2016. Formulation of the coupled electrochemical–mechanical boundary-value problem, with applications to transport of multiple charged species. Acta Mater. 104, 33–51.

Cabras, L., Danilov, D., Subber, W., Oancea, V., Salvadori, A., 2022. A two-mechanism and multiscale compatible approach for solid state electrolytes of (Li-ion) batteries. J. Energy Storage 48, 103842.

Cabras, L., Serpelloni, M., 2025. Electro-chemo-mechanics of solid state batteries: inelastic response to lithium plating and stripping. Proc. R. Soc. (Lond.) A 481 (2312), 20240230.

Carlstedt, D., Runesson, K., Larsson, F., Asp, L.E., 2022. On the coupled thermo–electro–chemo–mechanical performance of structural batteries with emphasis on thermal effects. Eur. J. Mech. A-Solid 94, 104586.

Castellani, E., Ismael, J., 2016. Which curie's principle? Philos. Sci. 83 (5), 1002–1013.

Castillo, J., Santiago, A., Judez, X., Garbayo, I., Coca Clemente, J.A., Morant-Miñana, M.C., Villaverde, A., González-Marcos, J.A., Zhang, H., Armand, M., Li. Safe, C., 2021. Flexible, and high-performing gel-polymer electrolyte for rechargeable lithium metal batteries. Chem. Mater. 33 (22), 8812–8821.

Chen, W., Zhao, Y.-P., 2022. Thermo-mechanically coupled constitutive equations for soft elastomers with arbitrary initial states. Int. J. Eng. Sci. 178, 103730.

Chester, S.A., 2012. A constitutive model for coupled fluid permeation and large viscoelastic deformation in polymeric gels. Soft Matter 8, 8223–8233.

Chester, S.A.., Anand, L., 2010. A coupled theory of fluid permeation and large deformations for elastomeric materials. J. Mech. Phys. Solids 58 (11), 1879–1906.

Chester, S.A., Anand, L., 2011. A thermo-mechanically coupled theory for fluid permeation in elastomeric materials: Application to thermally responsive gels. J. Mech. Phys. Solids 59 (10), 1978–2006.

Chester, S.A., Di Leo, C., Anand, L., 2015. A finite element implementation of a coupled diffusion-deformation theory for elastomeric gels. Int. J. Solids Struct. 52, 1–18.

Danilov, D., Notten, P.H.L., 2008. Mathematical modeling of ionic transport in the electrolyte of Li-ion batteries. Electrochim. Acta 53, 5569–5578.

De Groot, S.R., Mazur, P., 1984. Non-Equilibrium Thermodynamics. Dover.

Deb, D., 2024. Flexible polymerized ionic liquids gel polymer electrolytes for supercapacitor application. In: Bhowmik, Pradip K. (Ed.), Ionic Liquids. IntechOpen, Rijeka, (chapter 5).

Doi, M., 2009. Gel dynamics. JPSJ 78 (5), 052001.

Dreyer, W., Guhlke, C., Müller, R., 2016. A new perspective on the electron transfer: recovering the butler–volmer equation in non-equilibrium thermodynamics. Phys. Chem. Chem. Phys. 18 (36), 24966–24983.

Duda, F.P., Souza, A.C., Fried, E., 2010. A theory for species migration in a finitely strained solid with application to polymer network swelling. J. Mech. Phys. Solids 58 (4), 515–529.

Esmizadeh, S., Cabras, L., Serpelloni, M., Dev, T., Oancea, V., Knobbe, E., Lachner, M., Salvadori, A., 2024. A review on modeling of nucleation and growth of Li dendrites in solid electrolytes. J. Energy Storage 97, 112897.

Flory, P.J., 1942. Thermodynamics of high polymer solutions. J. Chem. Phys. 10 (1), 51–61.

Flory, P.J., Jr. Rehner, J, 1943. Statistical mechanics of cross-linked polymer networks II. Swelling. J. Chem. Phys. 11 (11), 521–526.

Ford, H.O., Park, B., Jiang, J.Z., Seidler, M.E., Schaefer, J.L., 2020. Enhanced Li^+ conduction within single-ion conducting polymer gel electrolytes via reduced cation-polymer interaction. ACS Mater. Lett. 2 (3), 272–279.

Ganser, M., Hildebrand, F.E., Kamlah, M., McMeeking, R.M., 2019. A finite strain electro-chemo-mechanical theory for ion transport with application to binary solid electrolytes. J. Mech. Phys. Solids 125, 681–713.
Gerdroodbar, A.E., Alihemmati, H., Safavi-Mirmahaleh, S.-A., Golshan, M., Damircheli, R., Eliseeva, S.N., Salami-Kalajahi, M., 2023. A review on ion transport pathways and coordination chemistry between ions and electrolytes in energy storage devices. J. Energy Storage 74, 109311.
Gurtin, M.E., Fried, E., Anand, L., 2010. The Mechanics and Thermodynamics of Continua. Cambridge University Press.
Gyftopoulos, E., Beretta, G.P., 2005. Thermodynamics: Foundations and Applications. Publications, New York.
Hajikhani, A., Wriggers, P., Marino, M., 2021. Chemo-mechanical modelling of swelling and crosslinking reaction kinetics in alginate hydrogels: A novel theory and its numerical implementation. J. Mech. Phys. Solids 153, 104476.
Han, S.Y., Lee, C., Lewis, J.A., Yeh, D., Liu, Y., Lee, H.-W., McDowell, M.T., 2021. Stress evolution during cycling of alloy-anode solid-state batteries. Joule 5 (9), 2450–2465.
Haohui, Z., Mohammad, D., Yuhang, H., 2020. Kinetics of polyelectrolyte gels. J. Appl. Mech. 7.
He, P., Chen, S., Choi, Y.Y., Myung, N.V., Nykaza, J.R., Schaefer, J.L., 2024. In-situ crosslinked gel polymer electrolytes based on ionic monomers as charge carriers for lithium-ion batteries. ECS Adv. 3 (1), 010504.
Holzapfel, G., 2001. Nonlinear Solid Mechanics: A Continuum Approach for Engineering. John Wiley & Sons, Ltd.
Hong, W., Zhao, X., Zhou, J., Suo, Z., 2008. A theory of coupled diffusion and large deformation in polymeric gels. J. Mech. Phys. Solids 56 (5), 1779–1793.
Huggins, M.L., 1942. Some properties of solutions of long-chain compounds. J. Phys. Chem. 46 (1), 151–158.
Jabbari, V., Yurkiv, V., Md G. Rasul, Tamadoni Saray, M., Rojaee, R., Mashayek, F., Shahbazian-Yassar, R., 2022. An efficient gel polymer electrolyte for dendrite-free and long cycle life lithium metal batteries. Energy Stor Mater. 46, 352–365.
Kaiser, T., Menzel, A., 2021. A finite deformation electro-mechanically coupled computational multiscale formulation for electrical conductors. Acta Mech. 232 (10), 3939–3956.
Kovetz, A., 1989. The Principles of Electromagnetic Theory. Cambridge University Press.
Latz, A., Zausch, J., 2015. Multiscale modeling of lithium ion batteries: thermal aspectst. Beilstein J. Nanotechnol. 6, 987–1007.
Li, Z., Fu, J., Zhou, X., Gui, S., Wei, L/., Yang, H., Li, H., Guo, X., 2023. Ionic conduction in polymer-based solid electrolytes. Adv. Sci. 10 (10), 2201718.
Liu, G., Lu, W., 2017. A model of concurrent lithium dendrite growth, SEI growth, SEI penetration and regrowth. J. Electrochem. Soc. 164 (9), A1826–A1833.
Lucantonio, A., Nardinocchi, P., Teresi, L., 2013. Transient analysis of swelling-induced large deformations in polymer gels. J. Mech. Phys. Solids 61 (1), 205–218.
McMeeking, R., Landis, C.M., 2005. Electrostatic forces and stored energy for deformable dielectric materials. J. Appl. Mech.-T ASME 72, 581–590.
Müller, W.H., Vilchevskaya, E.N., Eremeyev, V.A., 2022. Electrodynamics from the viewpoint of modern continuum theory—A review. ZAMM e202200179.
Narayan, S., Anand, L., 2022. A coupled electro-chemo-mechanical theory for polyelectrolyte gels with application to modeling their chemical stimuli-driven swelling response. J. Mech. Phys. Solids 159, 104734.
Narayan, S., Stewart, L., Anand, E.M., 2021. Coupled electro-chemo-elasticity: Application to modeling the actuation response of ionic polymer-metal composites. J. Mech. Phys. Solids 152, 104394.
Narayanan, P., Pramanik, R., Arockiarajan, A., 2023. A hyperelastic viscoplastic damage model for large deformation mechanics of rate-dependent soft materials. Eur. J. Mech. A/Solids 98, 104874.
Rossi, M., Nardinocchi, P., Wallmersperger, T., 2019. Swelling and shrinking in prestressed polymer gels: an incremental stress–diffusion analysis. Proc. R. Soc. (Lond.) A 475 (2230), 20190174.
Saito, Y., Stephan, A.M., Kataoka, H., 2003. Ionic conduction mechanisms of lithium gel polymer electrolytes investigated by the conductivity and diffusion coefficient. Solid State Ion 160 (1), 149–153.
Salvadori, A., Grazioli, D., Geers, M.G.D., 2015a. Governing equations for a two-scale analysis of Li-ion battery cells. Int. J. Solids Struct. 59, 90–109.
Salvadori, A., Grazioli, D., Geers, M.G.D., Danilov, D., Notten, P.H.L., 2015b. A multiscale-compatible approach in modeling ionic transport in the electrolyte of (Lithium ion) batteries. J. Power Sources 293, 892–911.
Salvadori, A., Grazioli, D., Magri, M., Geers, M.G.D., Danilov, D., Notten, P.H.L., 2015c. On the role of saturation in modeling ionic transport in the electrolyte of (Li-ion) batteries. J. Power Sources 294, 696–710.
Serpelloni, M., Cabras, L., Esmizadeh, S., Yildiz, E., Bastanfar, M., Valizadeh, N., Berlato, M., Salvadori, A., 2024. 4.14 - Mechanics of batteries. In: Silberschmidt, Vadim (Ed.), Comprehensive Mechanics of Materials, first ed. Elsevier, Oxford, pp. 335–354, first edition.
Shi, L., Yang, R., Lu, S., Jia, K., Xiao, C., Lu, T., Wang, T., Wei, W., Tan, H., Ding, S., 2018. Dielectric gels with ultra-high dielectric constant, low elastic modulus, and excellent transparency. NPG Asia Mater. 10 (8), 821–826.
Simo, J.C., Hughes, T.J.R., 1998. Computational Inelasticity. Springer-Verlag, New York.
Simon, A.M., Grzywna, Z.J., 1992. On the Larché-Cahn theory for stress-induced diffusion. Acta Metall. Mater. 40 (12), 3465–3473.
Song, S., Wang, J., Tang, J., Muchakayala, R., Ma, R., 2017. Preparation, properties, and Li-ion battery application of EC + PC-modified PVdF-HFP gel polymer electrolyte films. Ionics 23 (12), 3365–3375.
Tadmor, E.B., Miller, R.E., Elliott, R.S., 2011. Continuum Mechanics and Thermodynamics: From Fundamental Concepts to Governing Equations. Cambridge University Press.
Vernerey, F.J., Long, R., Brighenti, R., 2017. A statistically-based continuum theory for polymers with transient networks. J. Mech. Phys. Solids 107, 1–20.
Wang, X., Hong, W., 2012. A visco-poroelastic theory for polymeric gels. Proc. R. Soc. (Lond.) A 468 (2148), 3824–3841.
Wei, D., Shen, W., Xu, T., Li, K., Yang, L., Zhou, Y., Zhong, M., Yang, F., Xu, X., Wang, Y., Zheng, M., Zhang, Y., Li, Q., Yong, Z., Li, H., Wang, Q., 2022. Ultra-flexible and foldable gel polymer lithium–ion batteries enabling scalable production. Mater. Today Energy 23, 100889.
Xuanhe, Z., Wei, H., Zhigang, S., 2008. Stretching and polarizing a dielectric gel immersed in a solvent. Int. J. Solids Struct. 45 (14), 4021–4031.
Yildiz, E., Serpelloni, M., Salvadori, A., Cabras, L., 2024. A comparative review of models for all-solid-state li-ion batteries. Batteries 10 (5).
Zhu, M., Wu, S., Wang, Y., Song, M., Long, L., Hussain, S., Yang, X., Sui, G., 2019. Recent advances in gel polymer electrolyte for high-performance lithium batteries. J. Energy Chem. 37, 126–142.